WADC TECHNICAL REPORT NO. 55-88

March 1955

DEVELOPMENT OF A VARIABLE MACH NUMBER SLIDING BLOCK NOZZLE AND EVALUATION IN THE MACH NUMBER RANGE 1.3 TO 4.0

J. L. AMICK
H. P. LIEPMAN
T. H. REYNOLDS

University of Michigan

Engineering Research Institute Project No. 1951-13-F
Department of Aeronautical Engineering
Contract No. AF 33(038)-23070

United States Air Force
Wright Air Development Center
Air Research and Development Command
Wright-Patterson Air Force Base, Ohio

FOREWORD

This report was prepared by J. L. Amick, H. P. Liepman, and T. H. Reynolds of the Supersonic Wind Tunnel, Department of Aeronautical Engineering, University of Michigan, Ann Arbor, Michigan on Air Force Contract AF 33(038)-23070, under Expenditure Order No. 460-31-14. The work was administered under the direction of the Aeronautical Research Laboratory, Wright Air Development Center, with Dr. R. H. Mills acting as project engineer.

The contributions and assistance to this work of Professor A. M. Kuethe, Dr. J. S. Murphy, Dr. H. E. Bailey, Mr. R. P. Schulze, Mr. H. M. Emich, and the entire staff of the Supersonic Wind Tunnel of the University of Michigan are gratefully acknowledged.

ABSTRACT

A sliding-block wind tunnel nozzle was developed and tested in the Supersonic Wind Tunnel Facility of the University of Michigan at Mach numbers from 1.3 to 4.0. In this range the Mach number deviation from the average within a test rhombus is less than $\pm$ 0.9% and the flow angle deviation, less than $\pm$ 0.5°. The throat-to-test rhombus distance at the highest Mach number is 8.8 times the test-rhombus height. Overall pressure ratios required are about the same as those of conventional wind tunnels. The use of a curvature gage to control contour tolerances is discussed.

PUBLICATION REVIEW

The publication of this report does not constitute approval by the Air Force of the findings or the conclusions contained herein. It is published only for the exchange and stimulation of ideas.

For the Commander:

Leslie B. Williams, Colonel, USAF
Chief, Aeronautical Research Laboratory
Directorate of Research

TABLE OF CONTENTS

LIST OF FIGURES

LIST OF TABLES

NOMENCLATURE

a	Reflection thickness
A	Constant
B	Constant
C	Constant
D	Constant
d	Distance between y-axes of upper and lower contours
E	Young's modulus
G	Curvature gage reading
h	Distance between x-axes of upper and lower contours (Test section height)
I	Moment of inertia
l	Tang length
l_g	Gage length of curvature gage
l_j	Jack length
L	Wavelength of sine wave
M	Mach number
M_b	Bending moment
p	Static pressure
p_o	Stagnation pressure
p_o'	Pitot pressure
R	Radius of curvature
Re	Reynolds' number
S	Bending stress

T	Temperature
T_o	Stagnation temperature
t	Thickness
V	Shear force
x	Coordinates
y	
α	Flow angle
γ	Ratio of specific heats
Δ	Small, finite increment
δ^*	Displacement thickness
δ_T	Tang deflection
θ	Flow direction
K	Curvature
σ	Standard deviation
μ	Coefficient of viscosity
μ_o	Stagnation coefficient of viscosity
ν	Poisson's ratio

SECTION 1

INTRODUCTION

Variable Mach number nozzles have many potential advantages over the fixed-block type of nozzle for producing supersonic flow in wind tunnels. One promising type of variable nozzle, the asymmetric sliding-block type, has been shown to give good performance at Mach numbers below 3.0 (References 1-3). In order to extend the Mach number range of such a nozzle, the present investigation was begun early in 1951 under Air Force sponsorship. The objective was to determine contours of a sliding-block nozzle for the range M = 1.4 to 4.0, with experimental verification of satisfactory flow uniformity throughout the range. This final report presents the major results of the investigation, certain phases of which have already been covered in References 4-7.

SECTION 2

DEVELOPMENT OF NOZZLE CONTOURS

2.1 THEORETICAL CONTOURS

The nozzle contour design, given in detail in Reference 4, followed the iterative characteristic method outlined by Burbank and Byrne in Reference 3, with helpful suggestions by Dr. A. Ferri. Design Mach numbers of 1.64 and 3.87 were employed, and a throat test-section axis-inclination angle of 16° was used. Characteristic nets for intermediate Mach numbers of 2.37, 3.23, and 4.01 were also constructed. The following criteria were established to guide the construction of the characteristic nets:

1) The sonic line was to be straight and perpendicular to the nozzle contour.

2) No inflection points were to be used in the supersonic contours.

3) The first derivative of the contours was to be smooth and continuous.

4) No compression wavelets were to be employed.

Values of the second derivative along the contours were obtained by fairing and differentiating the slopes given by the characteristic nets. The second derivatives were then faired and integrated twice to obtain the contour coordinates. The subsonic portions were designed by one-dimensional theory, observing the requirement that the throat curvature should be essentially zero for 1 to 1-1/2 throat-heights upstream of the sonic line, in order to insure a straight, perpendicular sonic line.

An analytic method of design was subsequently developed and is given in Reference 5.

2.2 EXPERIMENTAL APPARATUS

2.2.1 Description of Nozzle.—A 4- by 4-inch model of the nozzle (Reference 6) was built in order to evaluate the theoretical contours and to make experimental corrections, if necessary. The nozzle was connected to the existing dry-air storage tank by entrance ducting and screens, and to the existing vacuum tank by an adjustable supersonic diffuser, fixed subsonic diffuser, and valves. The nozzle blocks consisted of flexible plates supported by jacks, with inflexible portions in the test section and subsonic region (Appendix A). In addition to the jack motion, each nozzle block could be rotated as a whole about a point near the throat. The sliding of the lower block to control Mach number was always in a direction parallel to the theoretical test-section axis, even with the block rotated. Plate glass windows measuring 8 by 41 inches extended from near the throat to about 4 inches downstream of the nozzle exit. Inflatable seals in grooves along the nozzle-block edges sealed the joints between the blocks and the windows or sideplates (Appendix B). An overall view of the tunnel with one side removed is shown in Fig. 2.1.

2.2.2 Pitot Rake.—Pitot pressures were measured with a five-prong, open-end rake. The prongs on the rake are 1-1/4 inches long and are spaced 1/2 inch apart. They are constructed of 17-gage (.058 OD, .042 ID) type-304 stainless steel hypodermic tubing, with the open end beveled 10° to a sharp inside edge. The body of the rake has a 2-1/4-inch span, 1/4-inch thickness, and 1-1/4 inch chord, with a sharp 45° edge at both leading and trailing edges, and it attaches to a 10-inch sting. A rack gear on this sting engages a pinion in the probe support (Reference 6), allowing the rake to be moved axially from outside the tunnel. Vertical position and angle of attack can also be changed during a run. Two set-screws in the body of the rake hold it to the sting at any angle of roll desired. Mercury manometers were used in conjunction with the pitot rake during both atmospheric and higher stagnation pressure runs.

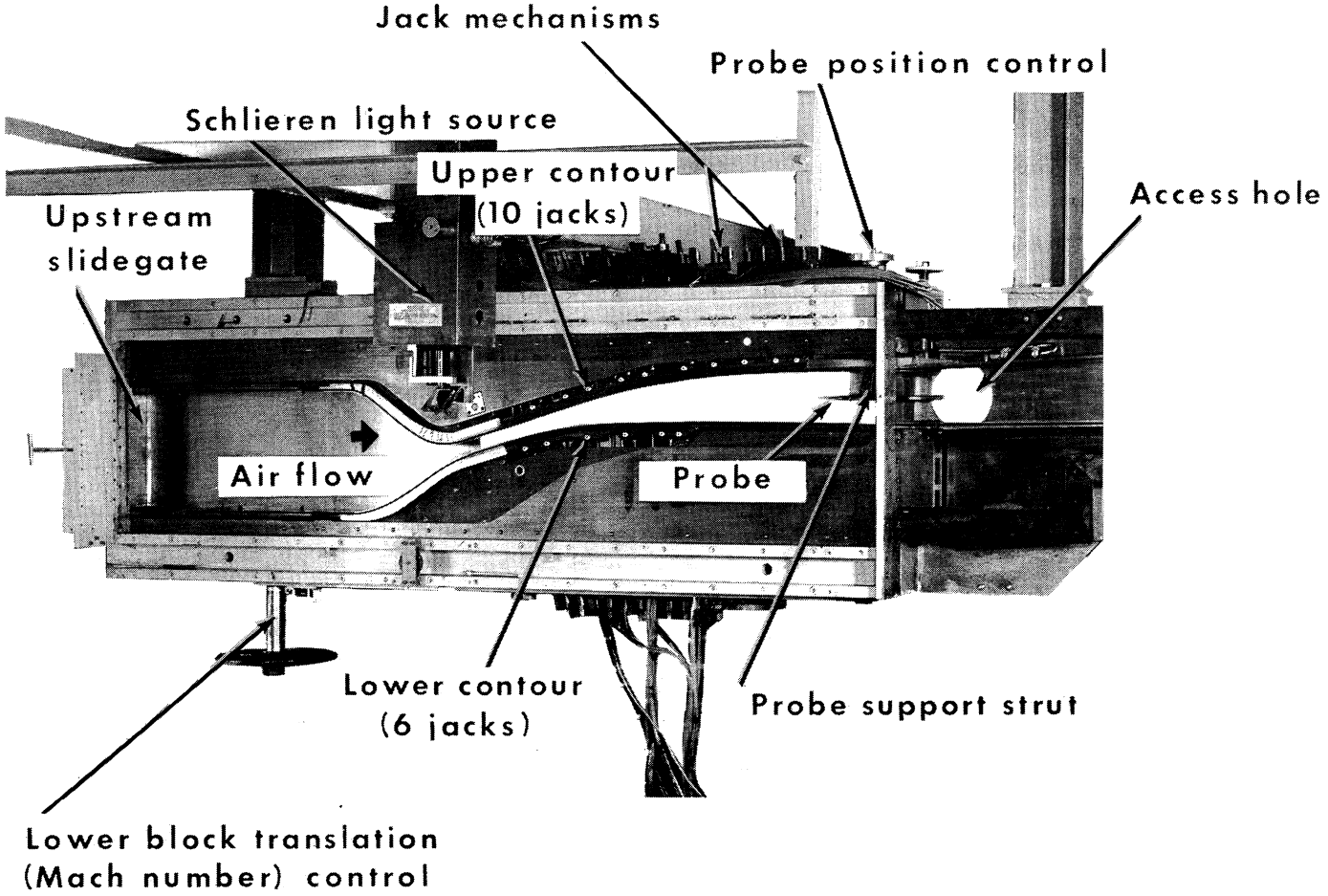

Fig. 2.1. View at nozzle with one side removed.

A similar three-prong pitot rake was used for some of the low Mach number work where the five-prong rake caused local blocking. A single pitot probe was also available.

2.2.3 Flow Inclinometer.—Flow inclination was measured with a wedge-type flow inclinometer. The flow inclinometer has five pairs of 0.042-inch diameter orifices spaced at 0.380-inch intervals spanwise, 0.350 inches from the leading edge. The plan form is rectangular, with a 2-inch span, 1/2-inch thickness, and 1-1/2-inch chord, and the wedge angle is 45° at both the leading and trailing edges. The flow inclinometer attaches to the probe support, thus enabling it to be moved axially, vertically, and to an angle of attack. The pressure differences between the orifices of each pair were measured by manometers using Meriam red oil of specific gravity 0.827. The sensitivity of these pressure differences to flow inclination was calibrated for each Mach number.

A second flow inclinometer, having a wedge angle of 12°, was available for use at low Mach numbers.

2.2.4 Static Orifices.—There are 24 1/32-inch-diameter static orifices along the lower nozzle contour, and 12 along the upper. Twenty of the lower-contour orifices lie along the straight portion of the block at 1-inch intervals. These static orifices were connected to manometer tubes filled with Meriam red oil. Only relative pressures were measured, because of the inconvenience of measuring absolute pressures with such a light fluid.

Static needle rakes were available but were not used because of the shock-free nature of the flow. It was reasoned that, in the absence of shocks, the flow through the nozzle should be essentially isentropic and, therefore, Mach numbers in the test section could be calculated from pitot and reservoir pressure measurements alone.

2.2.5 Schlieren System.—An 8-inch schlieren system was designed and built (Reference 7) for the purpose of qualitative analysis of the flow. This system proved to be useful for observation of starting and stopping shocks and boundary layer-probe shock interaction. However, the weak shock waves usually seen in schlieren pictures of supersonic flow were either absent or so weak as to be hidden by the mottled background produced by the commercial-quality surface finish on the plate glass windows.

2.3 TESTS AND RESULTS WITH THEORETICAL CONTOURS

For the first tests in the evaluation of the nozzle, the jacks were positioned so that the contours of each block by itself duplicated the theoretical inviscid contours. The flow produced by the nozzle was evaluated

with the pitot rake, flow inclinometer, and static orifices. The moving-probe technique (Appendix C) was also used. These measurements showed that the difference of extreme Mach numbers in a test rhombus 3.6 inches high varied between 1.6% at M = 1.5 and 3.8% at M = 3.2. The maximum difference in flow angle varied between 0.7° and 2.2° at the same Mach numbers. The major nonuniformity at all Mach numbers above 2.5 was a band of compression waves of about 1-1/2° total deflection angle, originating in (or reflecting from) the vicinity of the last three jacks on the upper contour.

No shock waves were detected in either the schlieren observations or the moving-probe tests. This absence of shock waves is attributed to the lack of physical junctures in the supersonic portion of the nozzle, and the lack of contour waviness of short wavelength.

In choosing the value 3.6 inches for the test rhombus height, it was assumed that Mach waves impinging on the boundary layer would curve as they entered the boundary layer, become normal to the wall, and reflect back along another curve to the outer edge of the boundary layer. As far as the reflected Mach wave is concerned, the process could be considered one of specular reflection from a "reflection" plane parallel to the wall within the boundary layer. In this and the following flow evaluations it was arbitrarily assumed that the reflection thickness (distance of this reflection surface from the wall) was 0.2 inches at all Mach numbers. This value represents about one-half to one-quarter of the boundary layer thickness, depending on the Mach number. The effective test rhombus height is then the actual height minus twice the reflection thickness.

2.4 IMPROVEMENT OF FLOW UNIFORMITY

2.4.1 Rotation.—The first change in nozzle configuration made to improve the flow uniformity consisted of an outward rotation of the downstream ends of both nozzle blocks, to effect a linear boundary layer correction. The changes in flow uniformity produced by this correction were small.

2.4.2 Sidewall Fences.—It was suspected that the flow nonuniformities might be caused at least partly by excessive thickening of the floor boundary layer due to downward flow in the sidewall boundary layers. The existence of flow from the sidewall boundary layers to the floor boundary layer was confirmed in tests utilizing the china clay method of visualization of boundary layer streamlines. Aluminum fences were then glued to the glass sidewalls, following the recommendations of Reference 8. Combinations of 3, 5, and 7 fences on each widewall were tested at M = 3.0. In each case the flow uniformity, as measured with the flow inclinometer, showed no improvement. There appeared, however, to be a reduction in boundary-layer cross flow as shown by china clay streamlines.

2.4.3 Upper Contour Correction.—Since the greatest flow nonuniformities occurred at the higher Mach numbers and consisted chiefly of a band of compression waves from the region of the last three jacks on the upper flexible plate, it appeared logical to attempt a correction by suitable repositioning of those jacks. This repositioning was done by trial-and error, and a combination of jack settings was found which reduced the compression band to one-quarter of its original strength. When this was tested at Mach numbers below 2.0, however, the flow was found to be less uniform than that produced by the original configuration in this Mach number range.

2.4.4 Boundary Layer Corrections.—Several different boundary-layer corrections were set into the contours by adjustment of the jacks. The first correction to be tried consisted of an outward movement of the contour at each station by an amount equal to the displacement thickness on the contour at that station. The displacement thicknesses were calculated by the Tucker method (Reference 9) for flow at M = 3.2, assuming zero boundary-layer thickness at the throat. The boundary layer thickness at the nozzle exit, calculated by this method, was in reasonable agreement with that obtained from pitot probe measurements of the actual boundary layer. The variation of boundary-layer displacement thickness in the test section was taken to be a straight line extension of that at the exit of the nozzle. Each jack was turned a certain number of revolutions calculated to move the contour a distance equal to the displacement thickness at that point.

The flow produced by the nozzle with this boundary-layer correction was measured with the pitot rake connected to mercury manometers. A definite improvement in flow uniformity was noted. The maximum Mach number variation within a 4-inch-high test rhombus was reduced to 2.6 percent or less over the whole Mach number range.

Next, the downstream ends of both nozzle blocks were rotated outward to make a linear correction for the sidewall boundary-layer displacement thickness in addition to that of the contoured walls. Due to mechanical limitations, however, only 0.9 of the sidewall displacement thickness at M = 3.2 could be corrected for. Tests with this nozzle setting showed only a slight improvement in uniformity over that of the two-wall correction. Due to the increased test-section height, a Mach number of 4.1 was reached with the lower block translated to its upstream limit; with the two-wall correction, the corresponding upper limit was a Mach number of 3.9.

Following the flow measurements, an accurate check on the actual nozzle contours was made by means of vernier height-gage measurements from a 48-inch Browne and Sharpe cast iron straightedge mounted on the side of the tunnel. At this time an error in rotation pin location was found. The vertical distance between the points of rotation of the two blocks was 0.028 inches greater than the theoretical value. The error amounts to a rotation

of one block with respect to the other by about 0.05 degrees. For any given Mach number, the distances between nozzle blocks at points between throat and test section are increased beyond the theoretical values by amounts up to 0.014 inches. Errors in the jack settings were also measured. These were probably due to lost motion and small deflections in the jack mechanisms.

In order to determine if removal of the above errors would further improve the flow, the contour was set accurately to the Tucker two-wall boundary-layer displacement thickness correction by means of the height gage and straightedge. This time the throat boundary-layer displacement thickness was assumed equal to 0.014 inches on each contour, thus taking up the extra 0.028-inch of throat height due to rotation pin misalignment. The resulting flow, however, showed about the same order of flow uniformity as that produced by the initial two-wall boundary-layer correction.

Since the above tests were made with the boundary-layer correction in the test section continued linearly from that in the nozzle, a calculation was made of the theoretical test-section displacement-thickness growth at $M = 3.2$, by the Tucker method. This calculation showed that the slope of the boundary-layer correction should be less in the test section than at the exit of the nozzle. The nozzle contours were therefore set to this more realistic boundary-layer correction by means of the straightedge and height gage. The flow uniformity, however, was made somewhat worse by this change.

2.4.5 Trial-and-Error Corrections.—In a search for further flow refinement, a trial-and-error method of contour correction was next tried. Starting with the two-wall boundary-layer correction, contour changes were made during a run by adjusting various jacks, and the effect on flow uniformity was observed on an oil manometer board which measured static pressures along the flat portion of the lower nozzle block. It is shown in Appendix D that the uniformity of flow in the test section of a two-dimensional nozzle can be determined directly from static pressure measurements along the floor or ceiling of the test section.

It was found that the flow could be made quite uniform at any given Mach number by adjusting the jacks during two or three runs. However, the flow at other Mach numbers would usually be worsened by this process. Although several methods of iteration were tried, no contour settings were found that would give a significant improvement throughout the Mach number range over the flow with the two-wall boundary-layer correction.

2.4.6 Final Correction.—The final contour setting was arrived at by going back to the two-wall Tucker displacement-thickness correction with test-section boundary-layer growth extrapolated linearly from that at the nozzle exit. This contour was accurately set by means of the height gage and straightedge. Some small changes were then made in the downstream part

of the upper contour, which improved the flow slightly at the higher Mach numbers, where the greatest nonuniformities had existed in the flow with unmodified boundary-layer correction. The flow produced by these final contours was then evaluated in great detail by means of pitot probe and static-wall pressure tests. The results of these tests, presented in Section 3, show a maximum Mach number variation within a 4-inch-high test rhombus of less than 1.6% at each Mach number tested in the range M = 1.3 to 4.0.

2.5 FINAL CONTOURS

The contours of the nozzle as finally adjusted were measured with the vernier height gage and cast iron straightedge. The measurements, when plotted as y-coordinate displacements from the theoretical contours, revealed a small amount of waviness having maximum amplitude midway between jacks. This waviness, which is believed to be an unavoidable consequence of supporting a flexible plate by a finite number of jacks, was eliminated by fairing a smooth curve through the measured points for each nozzle block. These final faired contours are shown in Fig. 2.2 in the form of displacements from the theoretical contours. The coordinates of the final faired contours are listed in Table 2.2, and those of the theoretical inviscid contours in Table 2.1. The deviations of the actual measurements from the faired contours are shown in Fig. 2.3.

Direct measurements of the curvature of the nozzle contours were made by means of the gage shown in Fig. 2.4. This gage, with the distances between the middle contact and the other two contacts set at 1/2-inch, reads directly one-quarter of the average curvature in the 1-inch interval (Appendix E). Measured values of the curvature of the contours are presented in Figs. 2.5 and 2.6 together with the curvature of the theoretical contours and of the faired contours.

Some of the curvature measurements plotted in Fig. 2.5 were made close to the edge of the flexible plate. Near each jack location these edge measurements depart from measurements made nearer the center, because the transverse curvature of the plate is restricted by the jack attachment, whose width is almost that of the plate.

SECTION 3

FLOW EVALUATION WITH FINAL CONTOURS

3.1 TESTS

3.1.1 Atmospheric Stagnation Pressure.—The flow produced by the

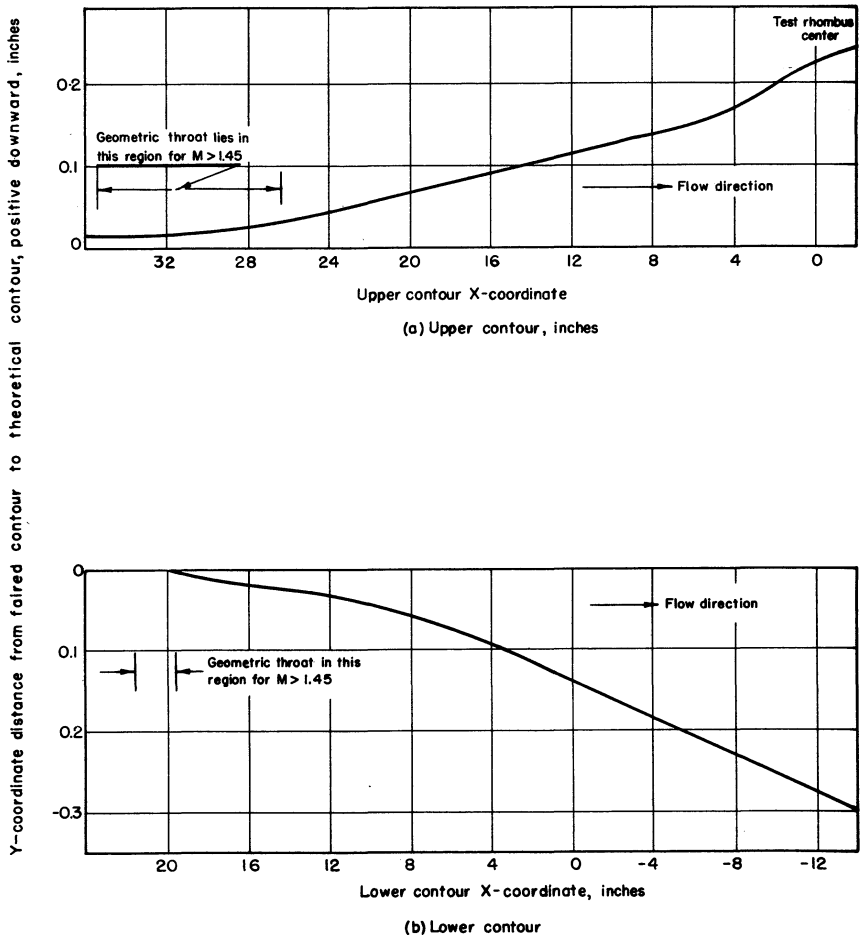

Fig. 2.2. y-coordinate difference between faired and theoretical contours.

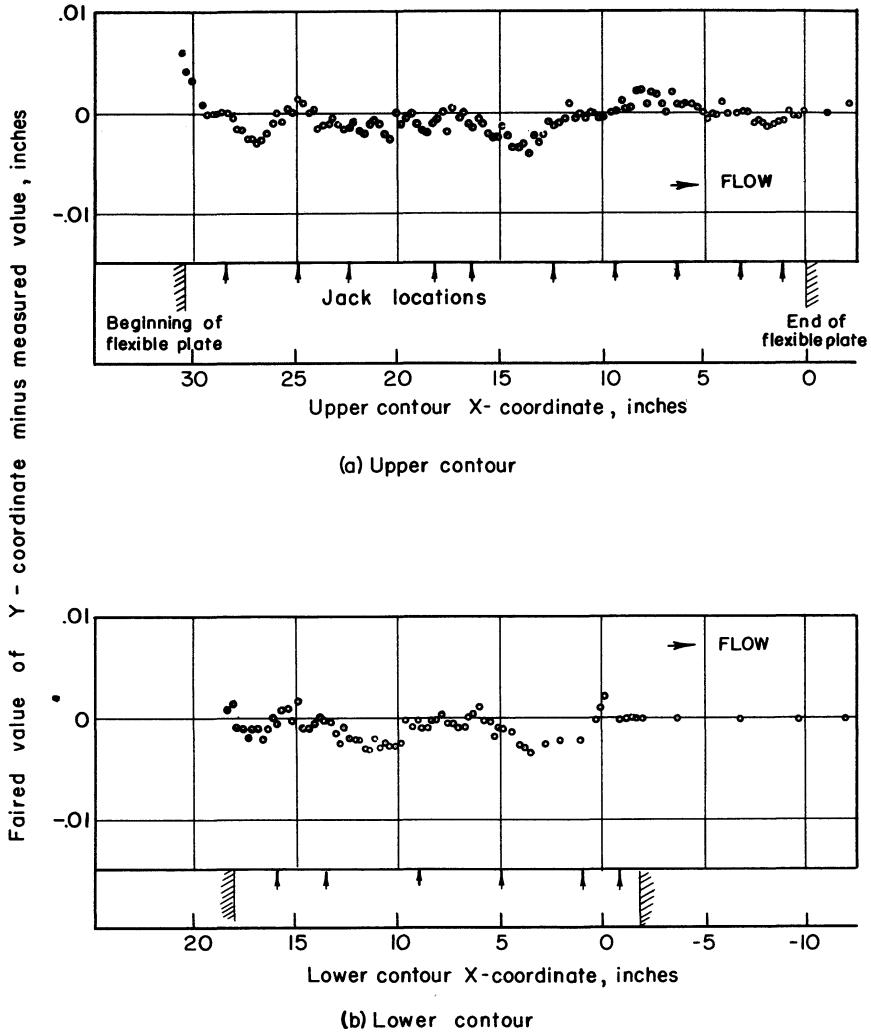

Fig. 2.3. Deviations of actual measurements from faired contours.

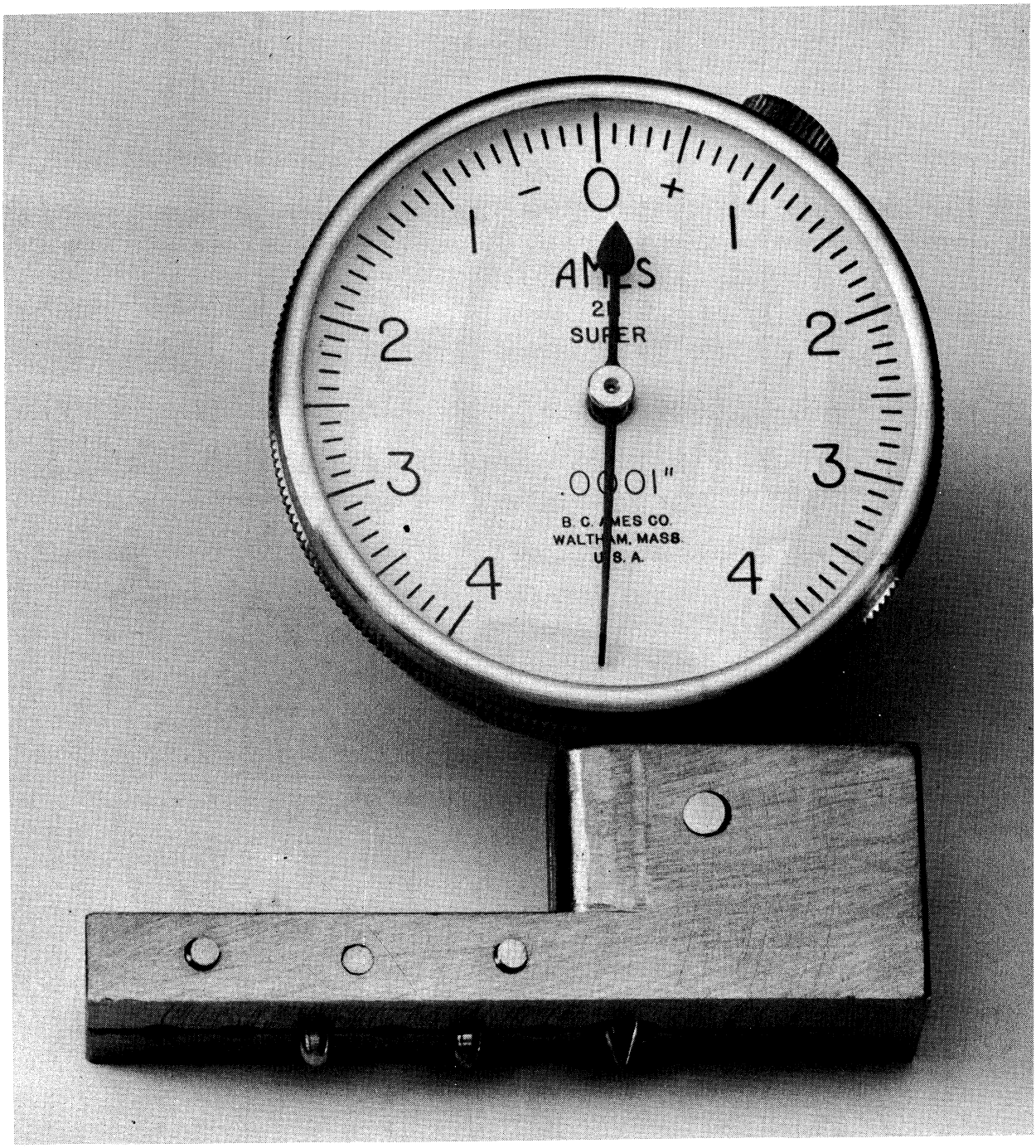

Fig. 2.4. Photo of curvature gage.

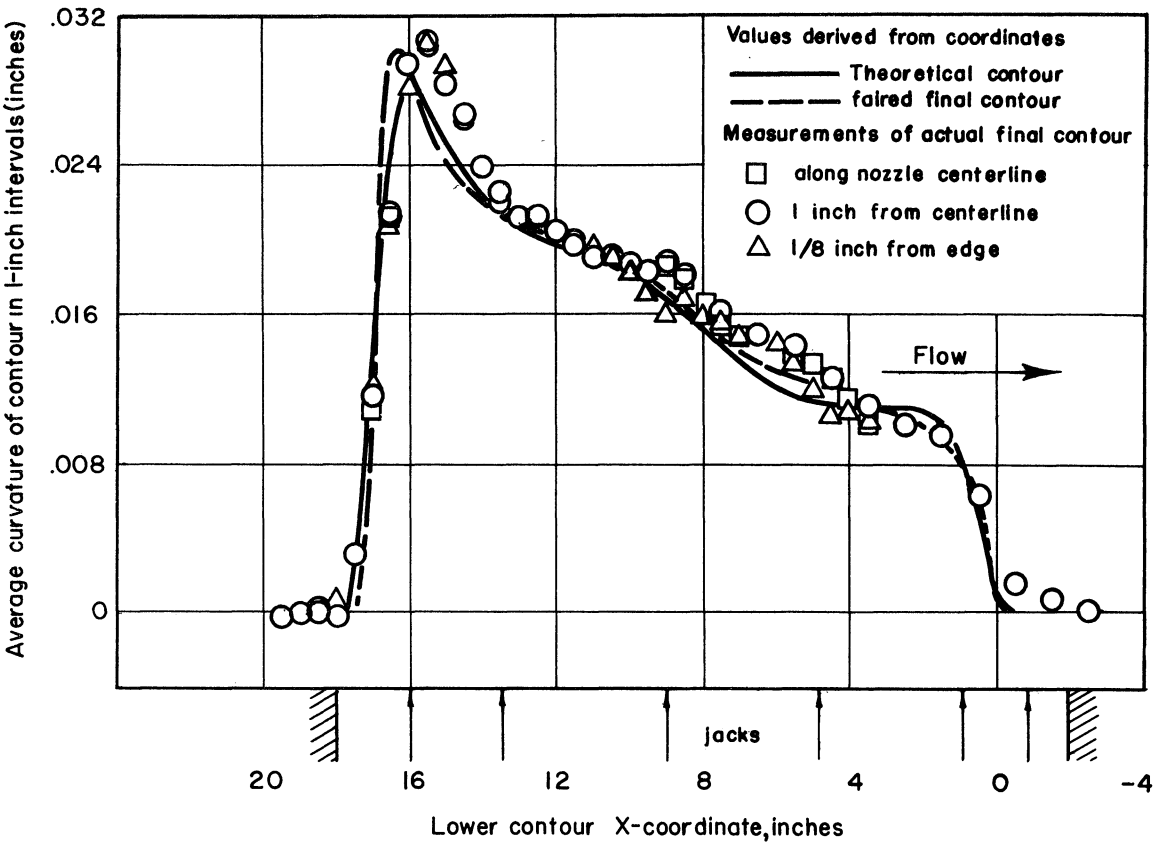

Fig. 2.5. Average curvature of lower contour in 1-inch intervals.

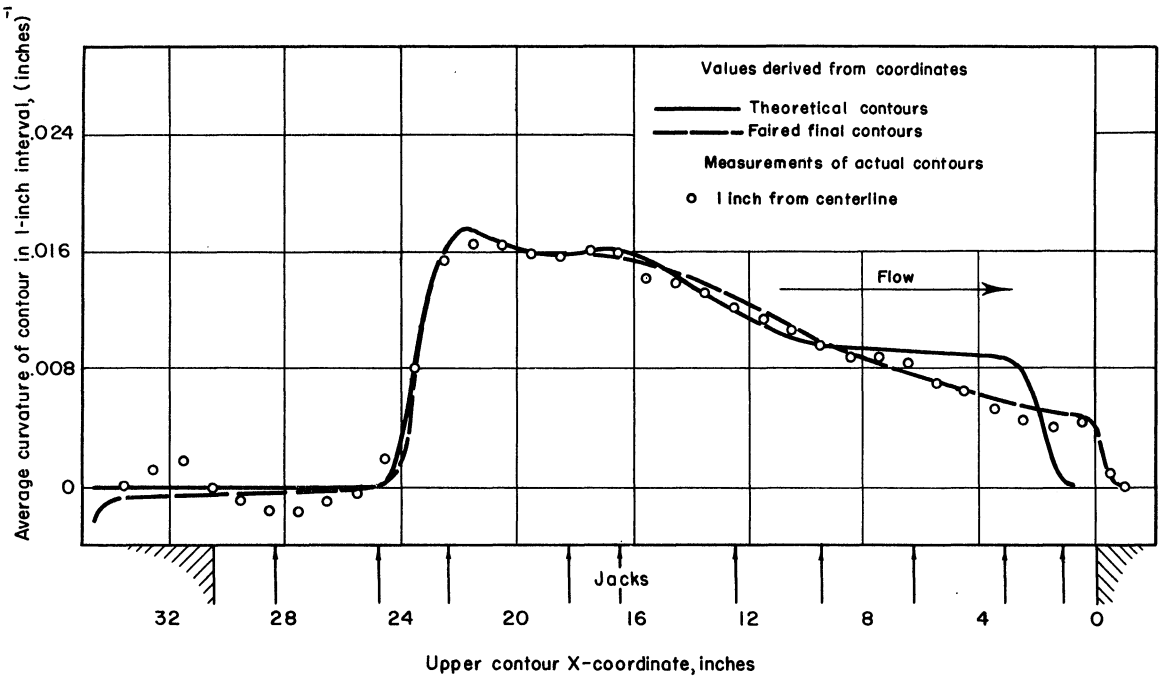

Fig. 2.6. Values of average curvature in 1-inch intervals for theoretical and final upper contours.

TABLE 2.1. COORDINATES OF THEORETICAL INVISCID CONTOURS

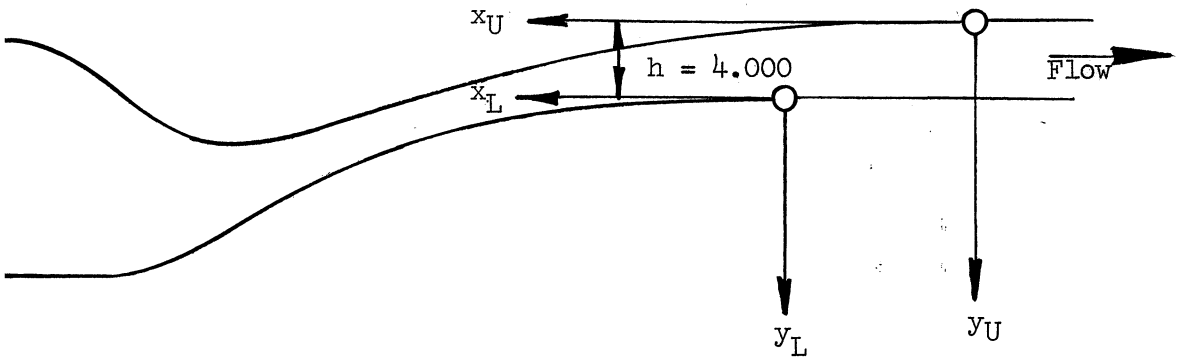

Lower Contour Coordinates

x_L	y_L	x_L	y_L	x_L	y_L	x_L	y_L
-12.00	0	8.75	.359	17.75	2.047	26.75	5.776
0	0	9.00	.384	18.00	2.119	27.00	5.938
0.25	0	9.25	.408	18.25	2.190	27.25	6.100
0.50	.001	9.50	.436	18.50	2.262	27.50	6.262
0.75	.001	9.75	.464	18.75	2.334	27.75	6.424
1.00	.002	10.00	.492	19.00	2.405	28.00	6.585
1.25	.003	10.25	.522	19.25	2.477	28.25	6.744
1.50	.005	10.50	.552	19.50	2.549	28.50	6.900
1.75	.008	10.75	.585	19.75	2.620	28.75	7.053
2.00	.011	11.00	.618	20.00	2.692	29.00	7.202
2.25	.015	11.25	.652	20.25	2.764	29.25	7.347
2.50	.019	11.50	.688	20.50	2.835	29.50	7.487
2.75	.024	11.75	.725	20.75	2.908	29.75	7.623
3.00	.030	12.00	.764	21.00	2.982	30.00	7.754
3.25	.036	12.25	.804	21.25	3.058	30.25	7.880
3.50	.043	12.50	.845	21.50	3.137	30.50	8.001
3.75	.052	12.75	.886	21.75	3.220	30.75	8.117
4.00	.060	13.00	.931	22.00	3.307	31.00	8.227
4.25	.069	13.25	.975	22.25	3.398	31.25	8.332
4.50	.079	13.50	1.021	22.50	3.493	31.50	8.431
4.75	.090	13.75	1.068	22.75	3.592	31.75	8.524
5.00	.101	14.00	1.117	23.00	3.695	32.00	8.612
5.25	.112	14.25	1.168	23.25	3.802	32.25	8.694
5.50	.125	14.50	1.219	23.50	3.913	32.50	8.770
5.75	.139	14.75	1.272	23.75	4.029	32.75	8.841
6.00	.153	15.00	1.328	24.00	4.150	33.00	8.906
6.25	.167	15.25	1.385	24.25	4.276	33.25	8.965
6.50	.183	15.50	1.423	24.50	4.408	33.50	9.018
6.75	.199	15.75	1.503	24.75	4.545	33.75	9.064
7.00	.216	16.00	1.565	25.00	4.687	34.00	9.101
7.25	.234	16.25	1.629	25.25	4.833	34.25	9.125
7.50	.252	16.50	1.695	25.50	4.983	34.50	9.135
7.75	.272	16.75	1.763	25.75	5.137	34.75	9.136
8.00	.293	17.00	1.833	26.00	5.294	35.00	9.136
8.25	.314	17.25	1.907	26.25	5.453		
8.50	.336	17.50	1.975	26.50	5.614		

TABLE 2.1 (cont'd)

Upper Contour Coordinates

x_U	y_U	x_U	y_U	x_U	y_U	x_U	y_U
-9.00	0	12.50	.525	25.25	3.107	38.00	6.481
0	0	12.75	.552	25.50	3.179	38.25	6.490
0.25	0	13.00	.578	25.75	3.251	38.50	6.490
0.50	0	13.25	.606	26.00	3.322	38.75	6.480
0.75	0	13.50	.634	26.25	3.394	39.00	6.461
1.00	0	13.75	.665	26.50	3.466	39.25	6.431
1.25	0	14.00	.695	26.75	3.538	39.50	6.391
1.50	0	14.25	.726	27.00	3.609	39.75	6.340
1.75	.001	14.50	.758	27.25	3.681	40.00	6.278
2.00	.001	14.75	.791	27.50	3.753	40.25	6.204
2.25	.002	15.00	.825	27.75	3.824	40.50	6.118
2.50	.003	15.25	.859	28.00	3.896	40.75	6.018
2.75	.004	15.50	.895	28.25	3.967	41.00	5.903
3.00	.007	15.75	.932	28.50	4.039	41.25	5.776
3.25	.009	16.00	.971	28.75	4.111	41.50	5.640
3.50	.013	16.25	1.010	29.00	4.183	41.75	5.497
3.75	.016	16.50	1.050	29.25	4.254	42.00	5.348
4.00	.020	16.75	1.091	29.50	4.326	42.25	5.194
4.25	.025	17.00	1.133	29.75	4.398	42.50	5.035
4.50	.031	17.25	1.176	30.00	4.469	42.75	4.872
4.75	.038	17.50	1.221	30.25	4.541	43.00	4.705
5.00	.045	17.75	1.266	30.50	4.613	43.25	4.534
5.25	.051	18.00	1.312	30.75	4.685	43.50	4.360
5.50	.060	18.25	1.360	31.00	4.756	43.75	4.183
5.75	.068	18.50	1.408	31.25	4.828	44.00	4.003
6.00	.076	18.75	1.458	31.50	4.900	44.25	3.821
6.25	.087	19.00	1.508	31.75	4.972	44.50	3.637
6.50	.097	19.25	1.559	32.00	5.043	44.75	3.452
6.75	.107	19.50	1.612	32.25	5.115	45.00	3.267
7.00	.119	19.75	1.666	32.50	5.186	45.25	3.083
7.25	.132	20.00	1.720	32.75	5.258	45.50	2.900
7.50	.144	20.25	1.776	33.00	5.330	45.75	2.720
7.75	.157	20.50	1.833	33.25	5.402	46.00	2.543
8.00	.171	20.75	1.891	33.50	5.473	46.25	2.370
8.25	.185	21.00	1.950	33.75	5.545	46.50	2.202
8.50	.199	21.25	2.011	34.00	5.616	46.75	2.040
8.75	.215	21.50	2.072	34.25	5.688	47.00	1.886
9.00	.231	21.75	2.135	34.50	5.760	47.25	1.742
9.25	.247	22.00	2.199	34.75	5.832	47.50	1.610
9.50	.265	22.25	2.264	35.00	5.903	47.75	1.493
9.75	.283	22.50	2.330	35.25	5.972	48.00	1.394
10.00	.302	22.75	2.398	35.50	6.039	48.25	1.315
10.25	.322	23.00	2.466	35.75	6.104	48.50	1.256
10.50	.342	23.25	2.536	36.00	6.166	48.75	1.215
10.75	.362	23.50	2.606	36.25	6.224	49.00	1.189
11.00	.383	23.75	2.677	36.50	6.278	49.25	1.175
11.25	.405	24.00	2.748	36.75	6.327	49.50	1.169
11.50	.427	24.25	2.821	37.00	6.371	49.75	1.167
11.75	.451	24.50	2.892	37.25	6.409	50.00	1.166
12.00	.475	24.75	2.964	37.50	6.440		
12.25	.499	25.00	3.036	37.75	6.464		

TABLE 2.2. COORDINATES OF FINAL CONTOURS

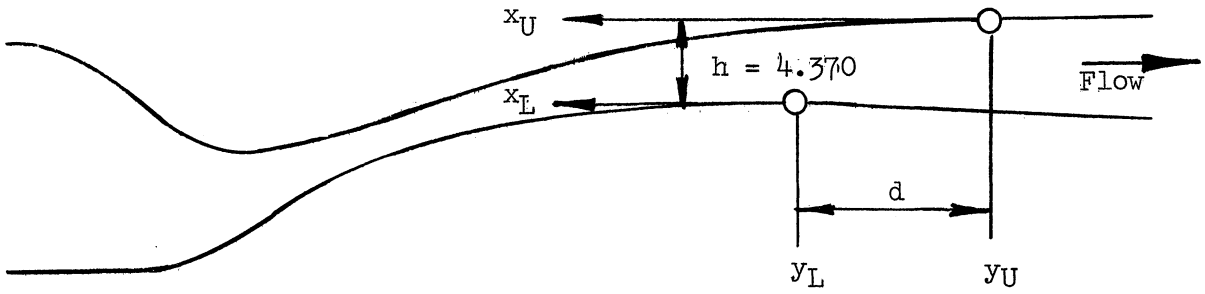

Lower Contour Coordinates							
x_L	y_L	x_L	y_L	x_L	y_L	x_L	y_L
-12.00	.1390	9.00	.2957	17.75	1.9200	26.50	5.440
0	0	9.25	.3195	18.00	1.9902	26.75	5.600
0.25	-.0029	9.50	.3444	18.25	2.0604	27.00	5.761
0.50	-.0056	9.75	.3704	18.50	2.1306	27.25	5.922
0.75	-.0079	10.00	.3976	18.75	2.2008	27.50	6.083
1.00	-.0097	10.25	.4260	19.00	2.2710	27.75	6.243
1.25	-.0110	10.50	.4556	19.25	2.3413	28.00	6.403
1.50	-.0118	10.75	.4864	19.50	2.4117	28.25	6.561
1.75	-.0120	11.00	.5184	19.75	2.4823	28.50	6.716
2.00	-.0116	11.25	.5516	20.00	2.5531	28.75	6.867
2.25	-.0106	11.50	.5861	20.25	2.623	29.00	7.014
2.50	-.0090	11.75	.6219	20.50	2.693	29.25	7.158
2.75	-.0067	12.00	.6590	20.75	2.764	29.50	7.298
3.00	-.0038	12.25	.6974	21.00	2.837	29.75	7.433
3.25	-.0002	12.50	.7371	21.25	2.912	30.00	7.564
3.50	+.0041	12.75	.7782	21.50	2.990	30.25	7.690
3.75	+.0091	13.00	.8206	21.75	3.071	30.50	7.810
4.00	+.0148	13.25	.8644	22.00	3.156	30.75	7.924
4.25	.0212	13.50	.9096	22.25	3.246	31.00	8.032
4.50	.0284	13.75	.9562	22.50	3.340	31.25	8.135
4.75	.0363	14.00	1.0042	22.75	3.438	31.50	8.232
5.00	.0450	14.25	1.0537	23.00	3.540	31.75	8.324
5.25	.0544	14.50	1.1047	23.25	3.646	32.00	8.411
5.50	.0646	14.75	1.1572	23.50	3.756	32.25	8.492
5.75	.0755	15.00	1.2113	23.75	3.870	32.50	8.567
6.00	.0872	15.25	1.2670	24.00	3.989	32.75	8.635
6.25	.0997	15.50	1.3244	24.25	4.114	33.00	8.697
6.50	.1130	15.75	1.3836	24.50	4.244	33.25	8.753
6.75	.1272	16.00	1.4447	24.75	4.380	33.50	8.803
7.00	.1422	16.25	1.5078	25.00	4.521	33.75	8.845
7.25	.1581	16.50	1.5730	25.25	4.666	34.00	8.878
7.50	.1749	16.75	1.6403	25.50	4.815	34.25	8.901
7.75	.1926	17.00	1.7095	25.75	4.967	34.50	8.913
8.00	.2112	17.25	1.7796	26.00	5.123	34.75	8.917
8.25	.2308	17.50	1.8498	26.25	5.281	35.00	8.917
8.50	.2514						
8.75	.2730						

Upper Contour Coordinates

x_U	y_U	x_U	y_U	x_U	y_U	x_U	y_U
9.00	-.0820	12.25	.6080	24.75	3.1533	37.25	6.624
0	0	12.50	.6348	25.00	3.2262	37.50	6.655
0.25	.0026	12.75	.6624	25.25	3.2991	27.75	6.679
0.50	.0055	13.00	.6909	25.50	3.3720	38.00	6.696
0.75	.0087	13.25	.7203	25.75	3.4449	38.25	6.705
1.00	.0122	13.50	.7506	26.00	3.5178	38.50	6.705
1.25	.0160	13.75	.7818	26.25	3.5907	38.75	6.695
1.50	.0201	14.00	.8139	26.50	3.6635	39.00	6.676
1.75	.0245	14.25	.8469	26.75	3.7363	39.25	6.646
2.00	.0292	14.50	.8808	27.00	3.8091	39.50	6.606
2.25	.0343	14.75	.9156	27.25	3.8818	39.75	6.555
2.50	.0397	15.00	.9514	27.50	3.9545	40.00	6.493
2.75	.0454	15.25	.9882	27.75	4.0272	40.25	6.419
3.00	.0515	15.50	1.0260	28.00	4.0998	40.50	6.333
3.25	.0579	15.75	1.0648	28.25	4.1724	40.75	6.233
3.50	.0647	16.00	1.1046	28.50	4.2450	41.00	6.118
3.75	.0719	16.25	1.1454	28.75	4.3175	41.25	5.991
4.00	.0795	16.50	1.1872	29.00	4.3900	41.50	5.855
4.25	.0875	16.75	1.2300	29.25	4.4625	41.75	5.712
4.50	.0959	17.00	1.2738	29.50	4.5349	42.00	5.563
4.75	.1047	17.25	1.3186	29.75	4.6073	42.25	5.409
5.00	.1139	17.50	1.3644	30.00	4.6797	42.50	5.250
5.25	.1235	17.75	1.4112	30.25	4.7520	42.75	5.087
5.50	.1335	18.00	1.4591	30.50	4.8243	43.00	4.920
5.75	.1439	18.25	1.5080	30.75	4.8965	43.25	4.749
6.00	.1548	18.50	1.5580	31.00	4.9687	43.50	4.575
6.25	.1662	18.75	1.6090	31.25	5.0409	43.75	4.398
6.50	.1781	19.00	1.6611	31.50	5.1130	44.00	4.218
6.75	.1905	19.25	1.7142	31.75	5.1851	44.25	4.036
7.00	.2034	19.50	1.7684	32.00	5.2571	44.50	3.852
7.25	.2168	19.75	1.8237	32.25	5.3291	44.75	3.667
7.50	.2307	20.00	1.8801	32.50	5.4010	45.00	3.482
7.75	.2451	20.25	1.9376	32.75	5.4729	45.25	3.298
8.00	.2601	20.50	1.9962	33.00	5.5447	45.50	3.115
8.25	.2756	20.75	2.0559	33.25	5.6165	45.75	2.935
8.50	.2917	21.00	2.1167	33.50	5.6882	46.00	2.758
8.75	.3083	21.25	2.1787	33.75	5.7599	46.25	2.585
9.00	.3255	21.50	2.2419	34.00	5.8315	46.50	2.417
9.25	.3433	21.75	2.3063	34.25	5.9031	46.75	2.255
9.50	.3617	22.00	2.3719	34.50	5.9746	47.00	2.101
9.75	.3807	22.25	2.4387	34.75	6.0460	47.25	1.957
10.00	.4004	22.50	2.5067	35.00	6.1170	47.50	1.825
10.25	.4207	22.75	2.5758	35.25	6.1867	47.75	1.708
10.50	.4417	23.00	2.6460	35.50	6.2545	48.00	1.609
10.75	.4633	23.25	2.7172	35.75	6.3194	48.25	1.530
11.00	.4856	23.50	2.7892	36.00	6.381	48.50	1.471
11.25	.5086	23.75	2.8618	36.25	6.439	48.75	1.430
11.50	.5323	24.00	2.9346	36.50	6.493	49.00	1.404
11.75	.5568	24.25	3.0075	36.75	6.542	49.25	1.390
12.00	.5820	24.50	3.0804	37.00	6.586	49.50	1.384
						49.75	1.382
						50.00	1.381

final contours was evaluated at M = 1.27, 1.34, 1.45, and 1.5 by means of floor static-pressure measurements, and at M = 1.6, 1.9, 2.5, 3.2 and 3.8 by pitot pressure measurements with the five-prong pitot rake. For most of the pitot tests the rake was mounted in the vertical roll position, and measurements were taken at a fixed height above the floor at axial stations spaced $0.5\sqrt{M^2 - 1}$ inches apart. Since the pitot orifices are 1/2 inch apart vertically, this axial spacing placed the orifices at the intersections of a network of equally spaced Mach lines. The pitot pressure measurements were made with mercury manometry, while static pressures were measured with Meriam red oil. The manometers were clamped near the end of each run and their heights read immediately afterward. All the tests were made at dewpoints below -25°F.

3.1.2 Higher Stagnation Pressure.—A limited number of runs was made at stagnation pressures of from 2 to 6 atmospheres in order to assess the effect of Reynolds' number variation on the nozzle performance. Fig. 3.1 shows the nozzle installation for the higher pressure tests. These tests were made at Mach numbers 1.9 and 3.2. Pitot pressures were measured at the same points in the flow as at atmospheric stagnation pressure, using similar instrumentation. The static pressure in the settling chamber was measured by two 100-inch Meriam mercury manometers in series, and converted to stagnation pressure through an experimental correction factor. Stagnation temperatures were recorded on a Brown recorder. Stagnation pressure was controlled manually by a Fischer valve which throttled the flow from about 400 psi to the desired stagnation pressure. The 400 psi air came, in turn, from a Foster reducing valve which was connected to a 3000 psi air storage tank. A bourdon-tube pressure transducer with an Atcotran pickup gave the operator a sensitive indication of stagnation pressure variations. The stagnation pressure variation during the ten seconds that the manometers were unclamped was usually less than 1/2%. The dewpoint of the air was always less than -25°F.

3.2 DATA REDUCTION

3.2.1 Method.—The pitot pressure data were reduced by a method based on the analysis in Appendix D. The data, as mentioned above, were taken at the points of intersection of a network of equally spaced upward-and downward-running Mach lines. Disturbance waves between two adjacent Mach lines produced a change in pitot pressure. The values of this change were obtained as the difference in pitot pressure ratio between a point on one line and a point on the other line lying on the same crossing Mach line. These difference values for a given pair of Mach lines were averaged in such a way that each measurement, where more than one measurement was made at a point, was given equal weight. These average difference values were then used in a plot showing the variation of pitot pressure ratio along a Mach line crossing the disturbances. This was done for the variation along both upward

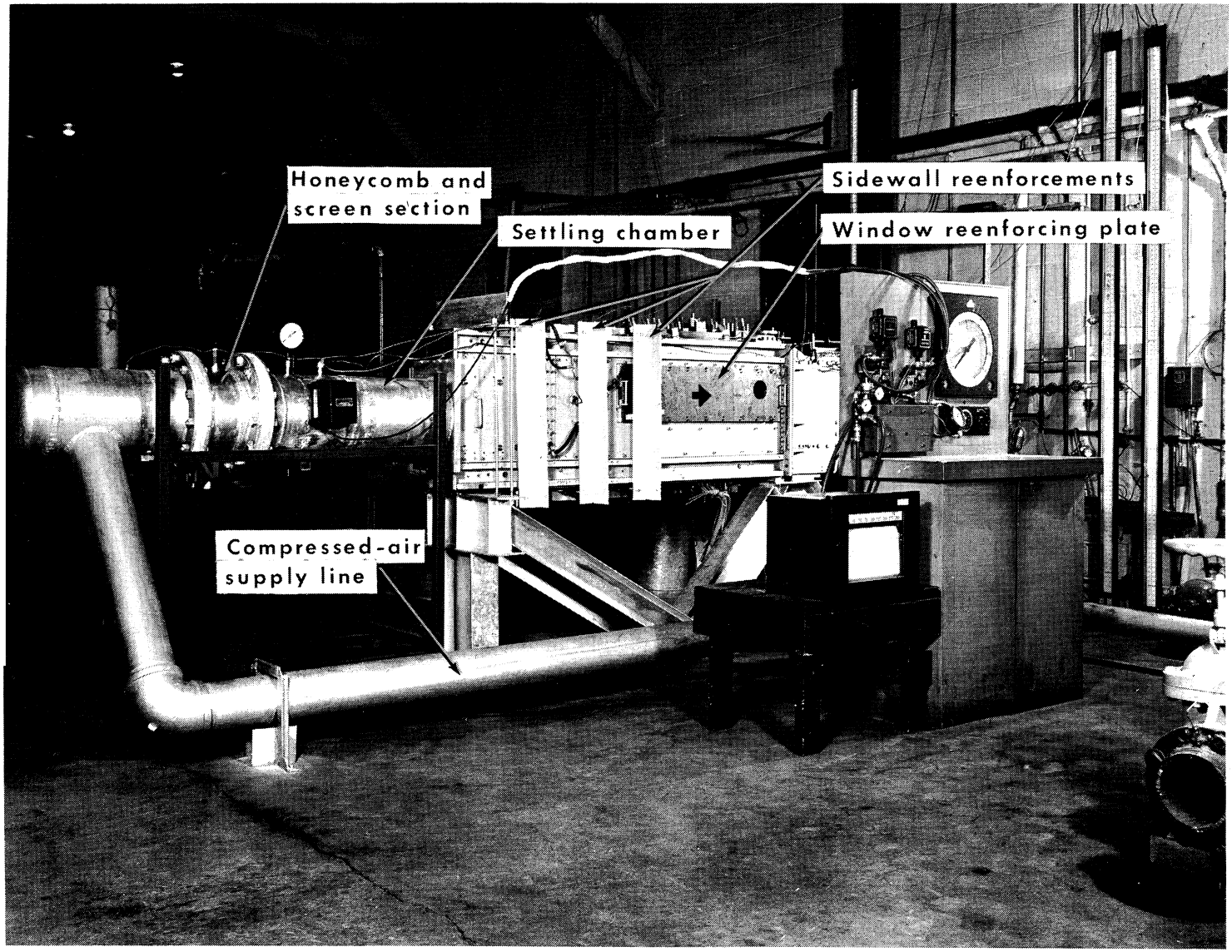

Fig. 3.1. Photo of nozzle installation for higher stagnation pressure tests.

and downward Mach lines, and then the two combined by reflection, assuming a 0.2-inch boundary-layer reflection thickness, to give the pitot pressure variation along a complete Mach line from floor reflection surface to ceiling reflection surface. A curve was faired through these points, and from it were read values of the faired difference in pitot pressure ratio between adjacent Mach lines of the network, along a crossing Mach line.

From the faired values of the difference in pitot pressure ratio between Mach lines of the network, a set of faired values of pitot pressure ratio, one value for each point of the network, was constructed. This set of faired values was chosen so that the overall average of the differences, between faired and measured values at a point, equaled zero. These faired values are considered to be the best estimates of the true values at the points of measurement that can be deduced from all the data considered as a whole, consistent with the assumptions of Appendix D.

The pitot pressure ratios were converted to Mach numbers with the assumption of isentropic flow through the nozzle. The method of Appendix D was then used to find the variation of flow uniformity as a function of rhombus axial location. A fixed position of the test rhombus was chosen as a compromise between best flow uniformity over the Mach number range and minimum nozzle length. At each Mach number the Mach number distributions along the sides of the rhombus at this location were integrated, and the average Mach number within the rhombus was obtained. The maximum plus and minus deviations from the average within the rhombus were then found. The same steps were followed to obtain the flow-angle deviation from the average.

3.2.2 Accuracy.—An indication of the accuracy of the data reduction procedure is given in Fig. 3.2. This figure presents the standard deviation of the measured values from the faired (average) values as a function of Mach number. Also plotted for comparison is the expected standard deviation due to experimental error only, as determined by statistical analysis of repeat data. These values of standard deviation are in terms of pitot pressure ratio. For convenience in converting to Mach number or flow angle the magnitudes of the deviation in pitot pressure ratio associated with 0.1% change in Mach number and 0.05° change in flow inclination are also shown.

Another comparison between the measured values of pitot pressure ratio and the faired values is presented in Figs. 3.3 and 3.4. These figures show the faired pressure-ratio variation along Mach lines through the points of measurement, together with the measured values. The scales have been stretched linearly for ease of plotting. It should be noted that in accordance with theory, the difference in faired values of the pressure ratio between any two Mach lines of a given family along a crossing Mach line is a constant.

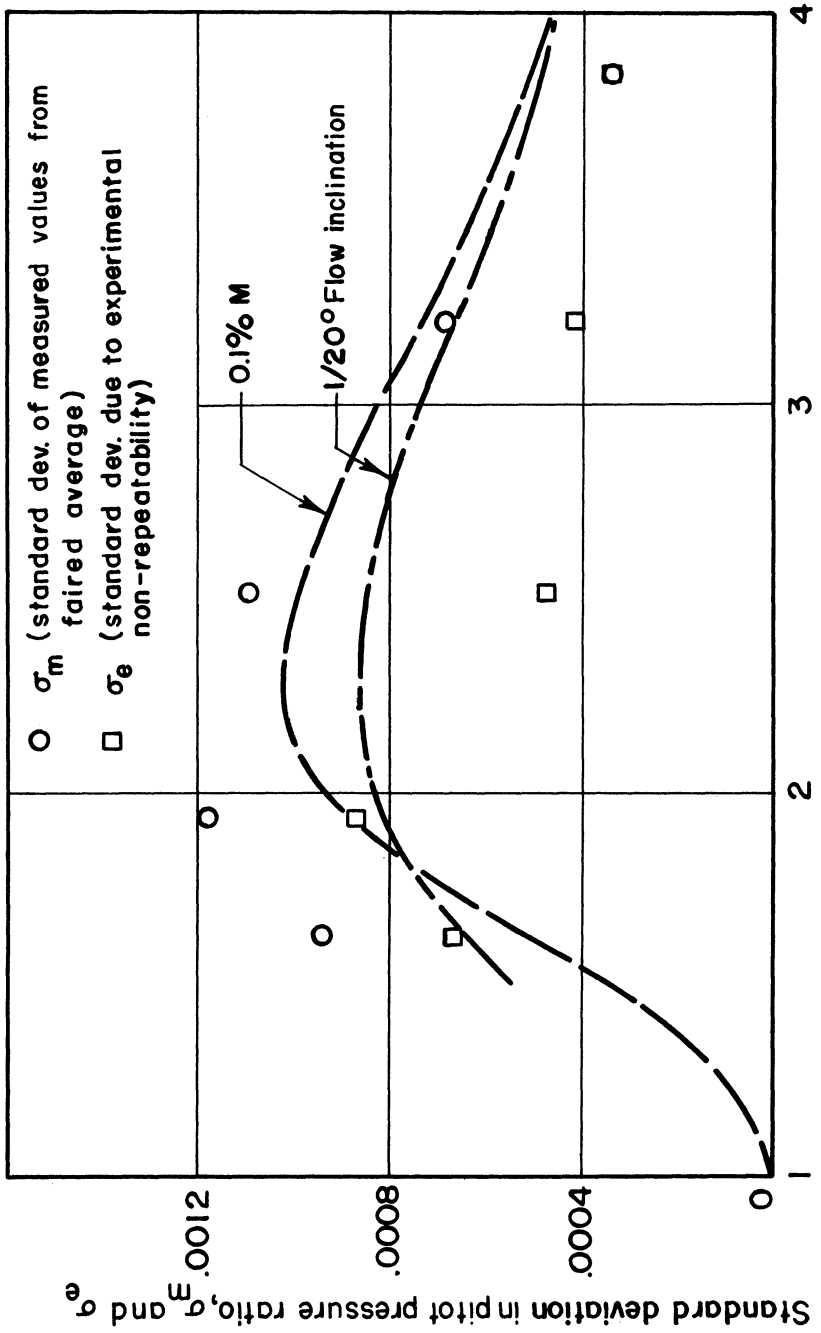

Fig. 3.2. Standard deviation of pitot pressure measurements from faired values. Tests at atmospheric stagnation.

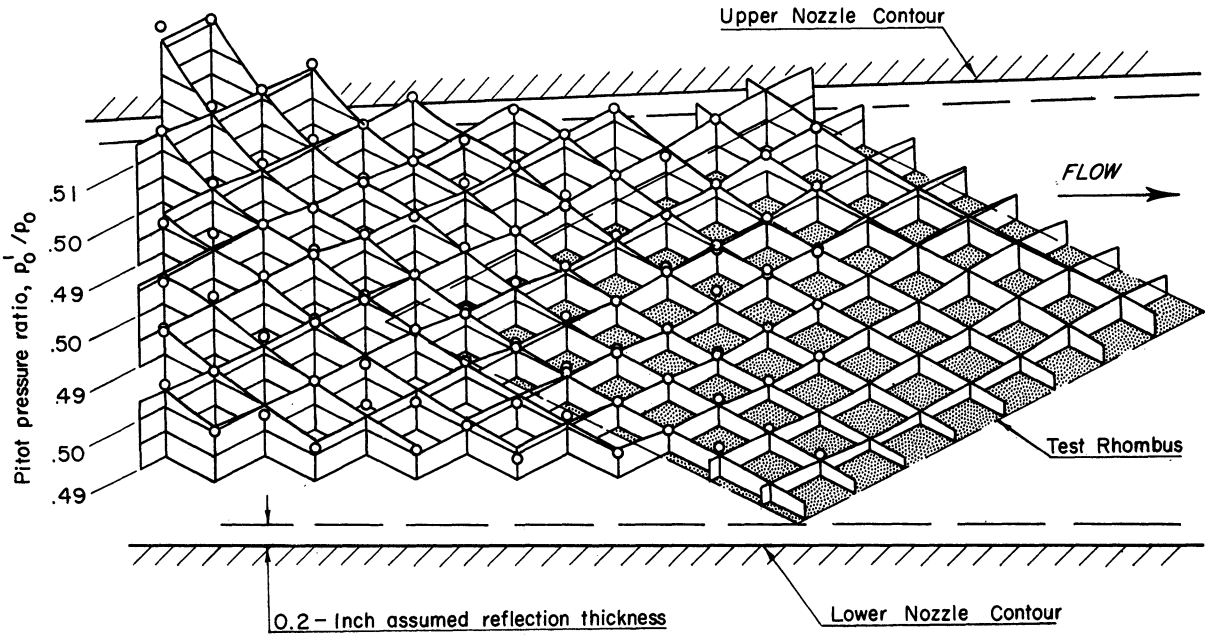

Fig. 3.3. Comparison of faired pitot-pressure distribution with the data points. M = 2.51.

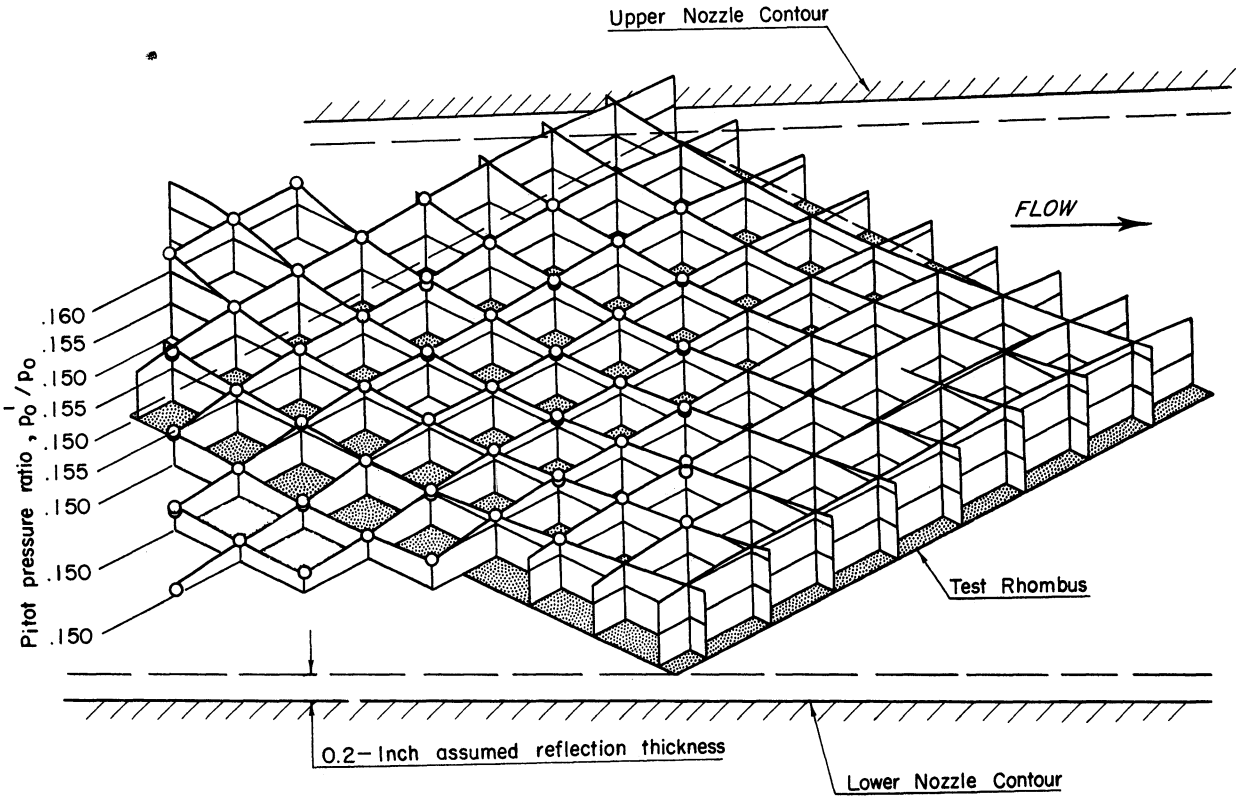

Fig. 3.4. Comparison of faired pitot-pressure distribution with the data points. M = 3.84. Atmospheric stagnation.

3.2.3 Two Dimensionality.—The results given above were obtained in the vertical center plane of the tunnel and reduced by a process which assumes two-dimensional flow. The validity of this assumption was checked by measurements made with the five-prong pitot rake in a horizontal attitude. At most locations of the rake the agreement of the five measurements was very good. The greatest deviation between measurements along any transverse line was about 0.2% in Mach number. This occasional slight non-two-dimensionality may account for the increase of the standard deviation over that given by the experimental errors in Fig. 3.2.

3.2.4 Details.—Details of some steps in the data evaluation process are shown in Figs. 3.5 to 3.10. Fig. 3.5 shows the static-pressure distribution along the floor of the test section at M = 1.27, 1.34, 1.45, and 1.51. As the static-pressure measurements were relative, the average Mach number values shown here were obtained by extrapolation of pitot pressure measurements at M = 1.6 and above. Each curve covers one complete cycle of the pressure variation along the floor.

Figs. 3.6 to 3.10 show the variation of pitot pressure ratio along the exit Mach line (the upward-running Mach line intersecting the upper contour at the nozzle end). In these figures the difference in value between adjacent points of like symbol represents the average of the pitot-pressure ratio changes measured between Mach lines which cross the exit Mach line at the height shown. The points at the ends of a series of like symbols were not given as much weight in fairing as those nearer the middle, since they represent the averages of only a few measurements. Data from floor static-pressure measurements are also included in Figs 3.7 and 3.8, converted to pitot-pressure ratio variation along the Mach lines.

The Mach number variation along the nozzle exit Mach line is shown in Fig. 3.11 for each of the nine Mach number settings. From this figure the maximum Mach number variation within a test rhombus was obtained as a function of rhombus axial location, for each nominal Mach number, as shown in Fig. 3.12. This figure shows that movement of the test rhombus downstream of the nozzle exit would result in only a slight improvement of the flow uniformity at those Mach number settings where the flow is already most uniform. The flow at the least uniform Mach number settings would not be improved. Therefore, it was decided to present the flow calibration data in terms of a test rhombus at the nozzle exit in order to keep the throat-to-test-rhombus length as small as possible.

3.3 RESULTS

3.3.1 Flow Uniformity.—The main calibration results with the final contours are summarized in Fig. 3.13 and are presented in greater detail in Figs. 3.14 to 3.22. Fig. 3.13 shows the maximum plus and minus deviations of

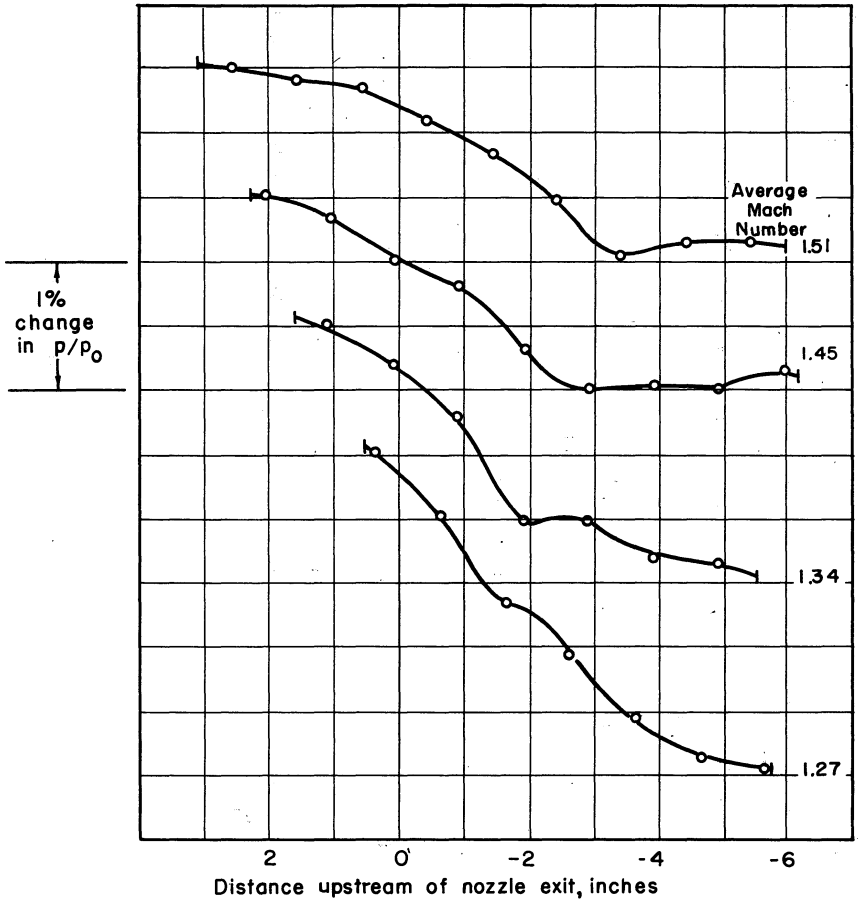

Fig. 3.5. Static pressure distribution along floor of test section at M = 1.27, 1.34, 1.45, and 1.51. Atmospheric stagnation.

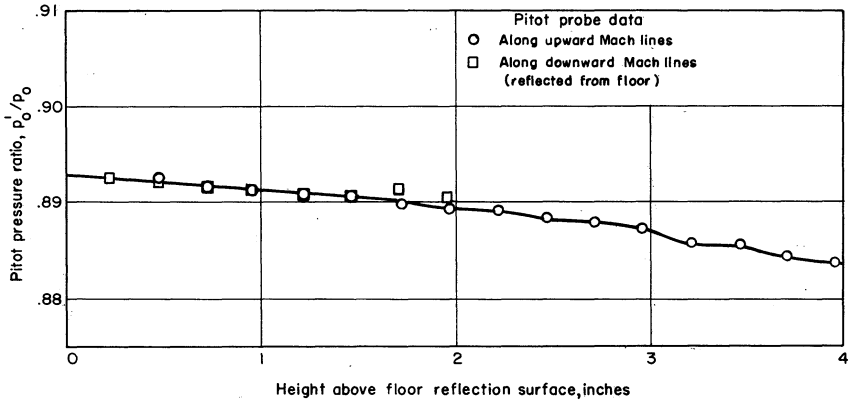

Fig. 3.6. Pitot-pressure ratio distribution along exit Mach line at M = 1.63. Atmospheric stagnation.

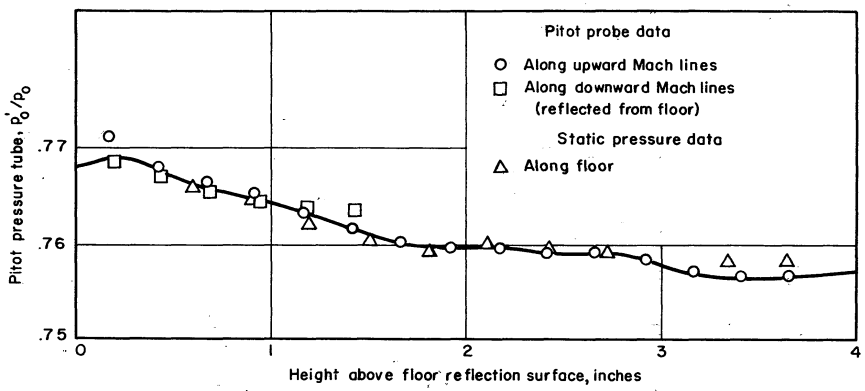

Fig. 3.7. Pitot-pressure ratio distribution along exit Mach line at M = 1.93. Atmospheric stagnation.

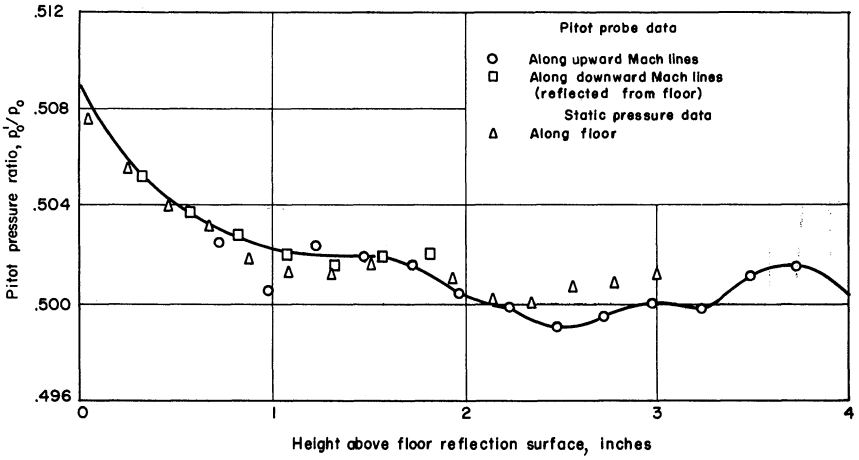

Fig. 3.8. M = 2.51

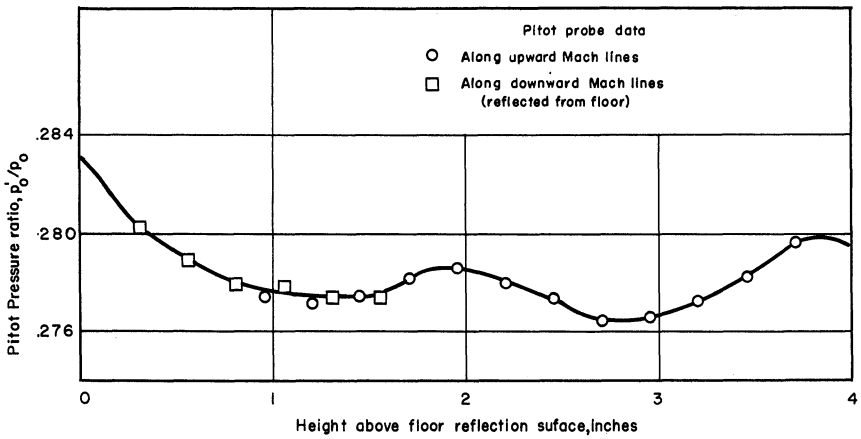

Fig. 3.9. M = 3.21

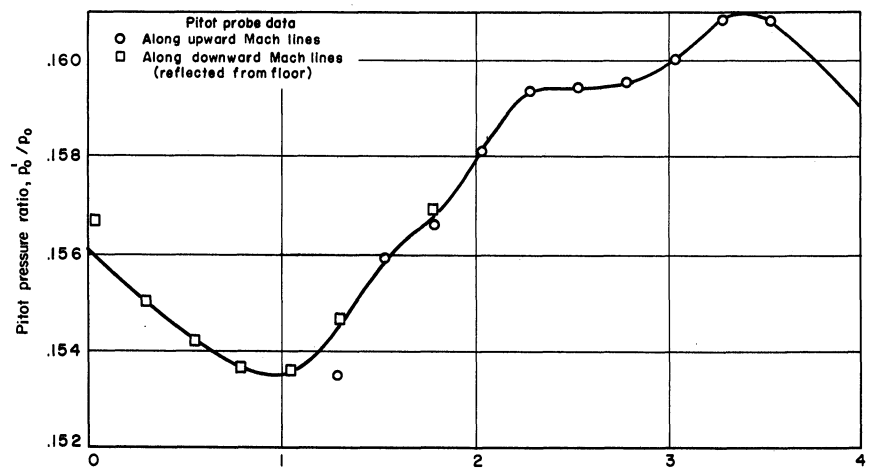

Fig. 3.10. M = 3.84

Pitot-pressure ratio distribution along exit Mach line. Atmospheric stagnation.

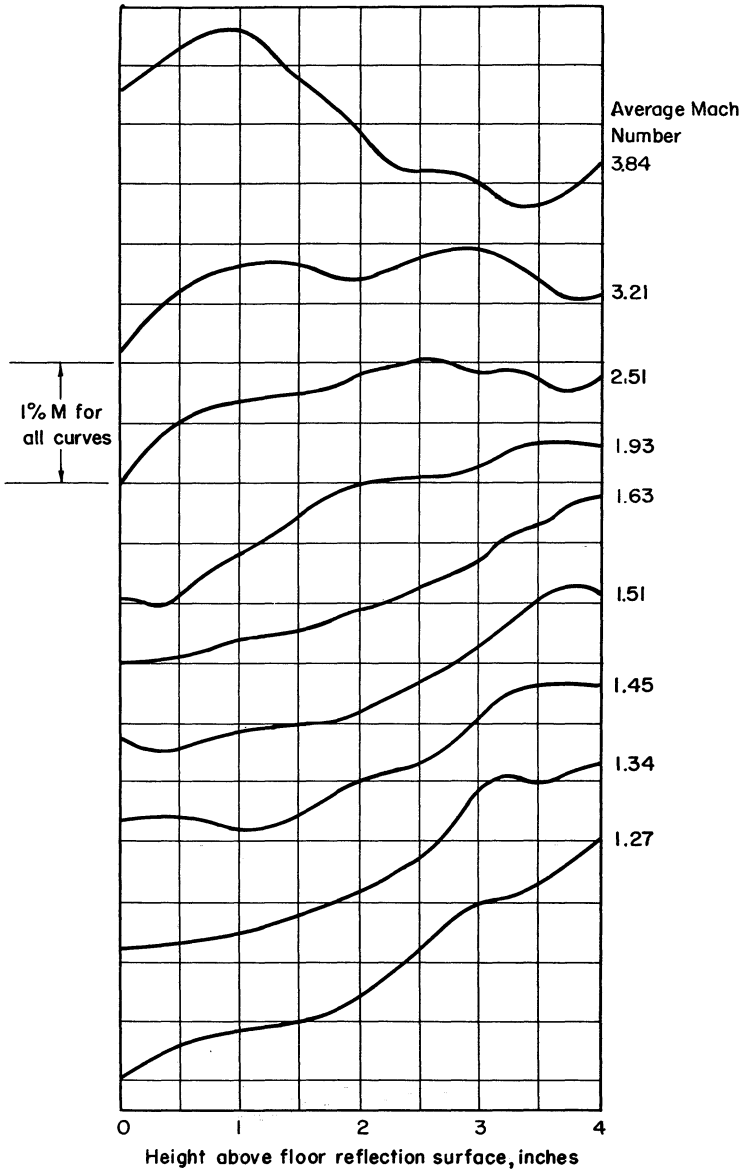

Fig. 3.11. Mach number distribution along nozzle exit Mach line.

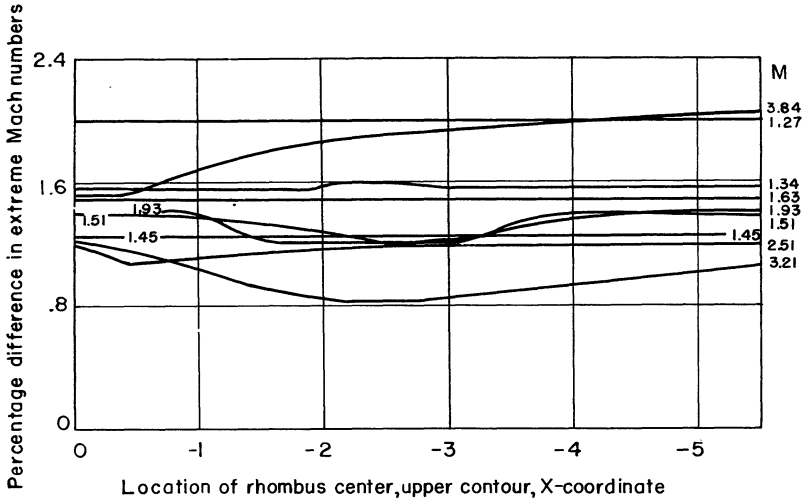

Fig. 3.12. Effect of rhombus location on difference of extreme Mach numbers in rhombus.

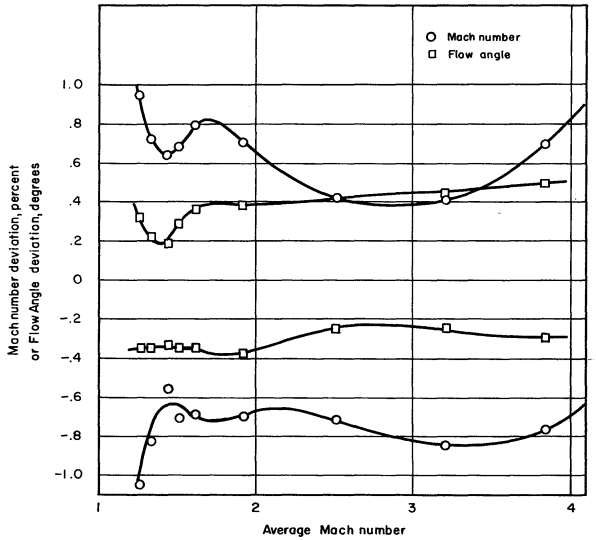

Fig. 3.13. Maximum deviations of Mach number and flow angle from average within a 4-inch high test rhombus centered at the nozzle exit.

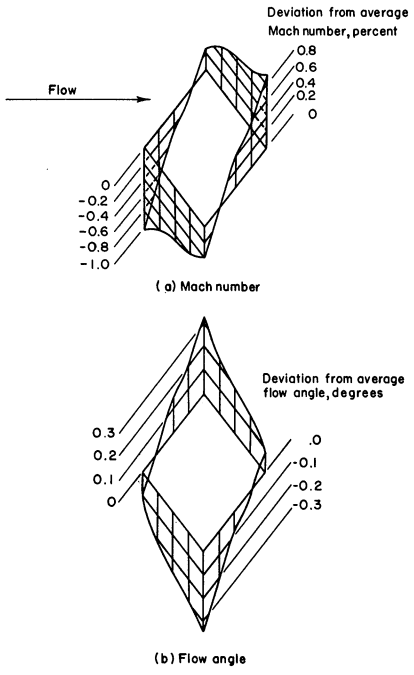

Fig. 3.14. M = 1.27

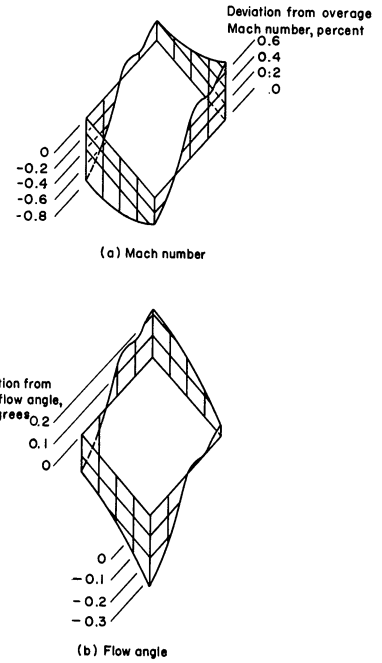

Fig. 3.15. M = 1.34

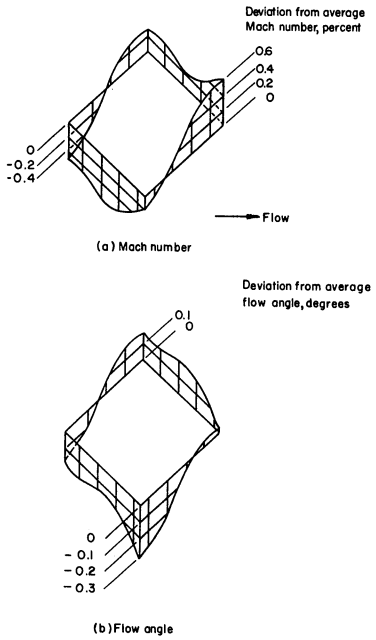

Fig. 3.16. M = 1.45

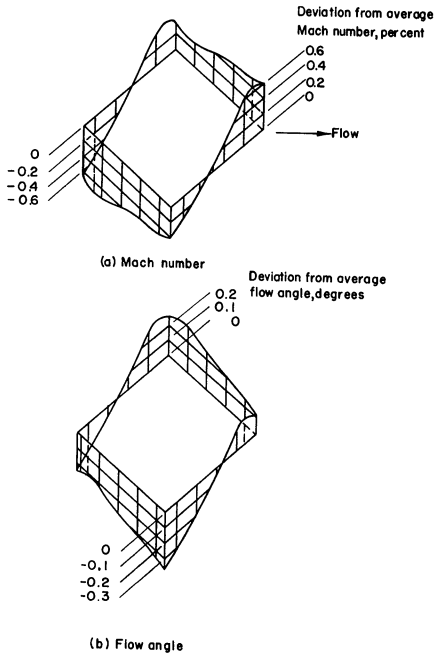

Fig. 3.17. M = 1.51

Mach number and flow-angle variation
along test-rhombus perimeter.

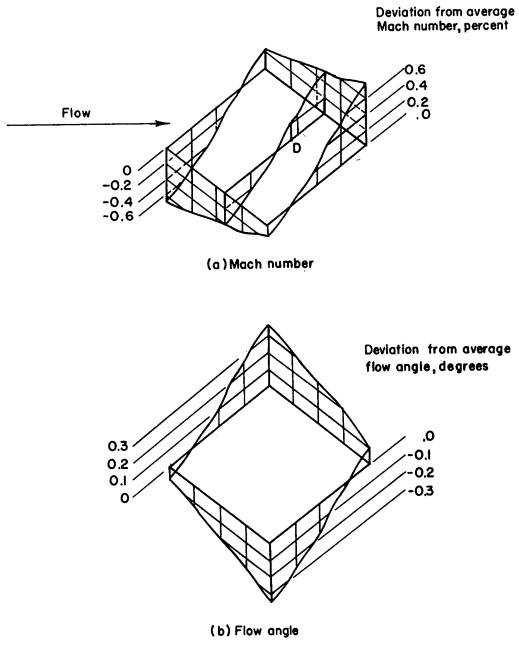

Fig. 3.18. M = 1.63

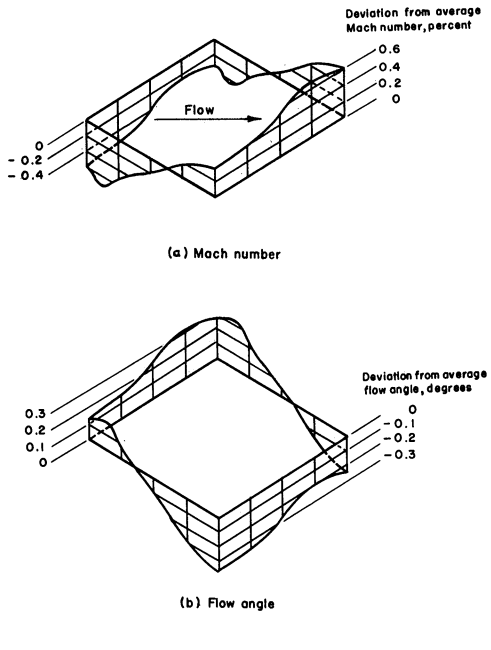

Fig. 3.19. M = 1.93

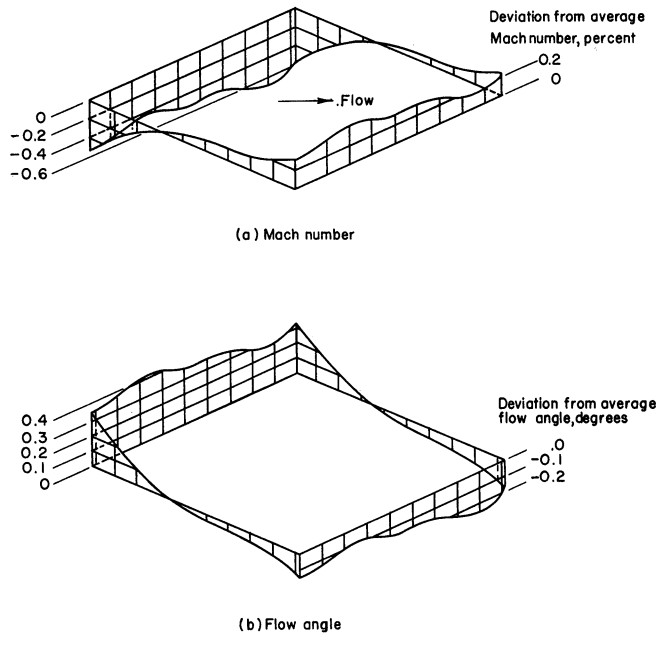

Fig. 3.20. M = 2.51

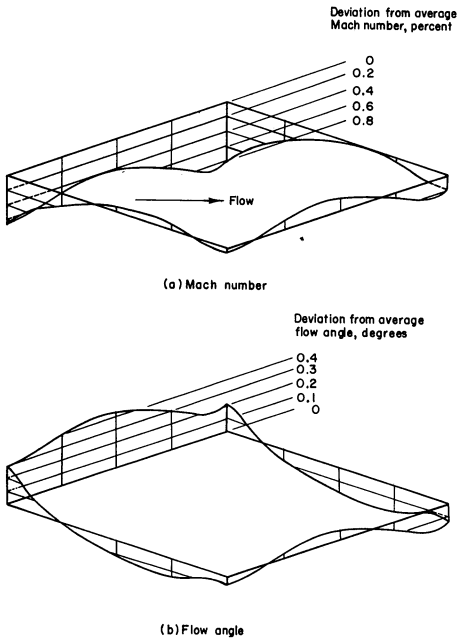

Fig. 3.21. M = 3.21

Mach number and flow-angle variation
along test-rhombus perimeter.

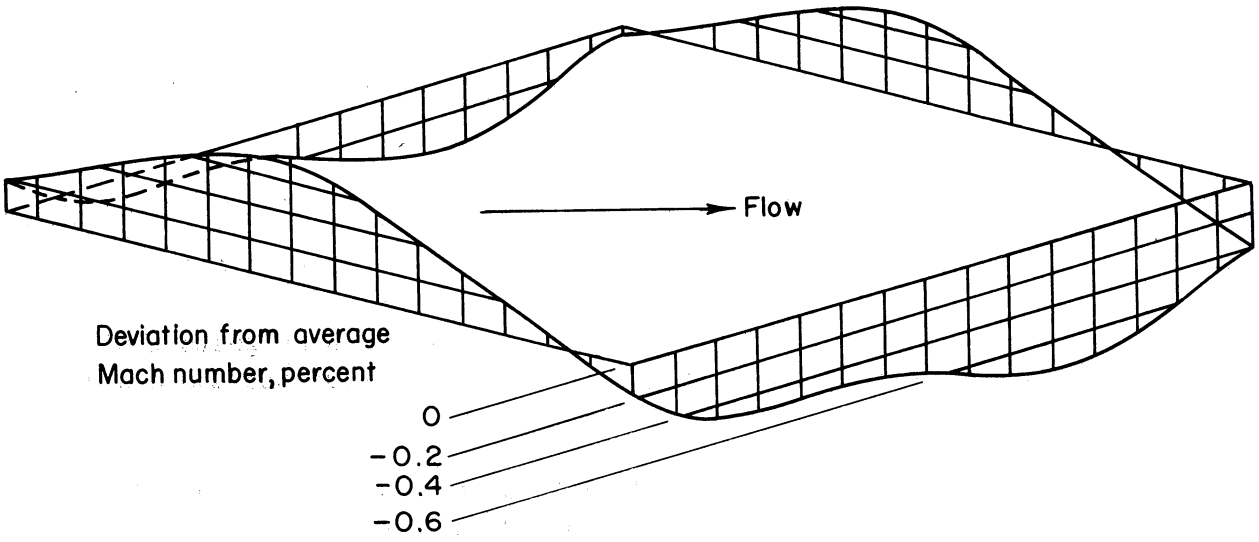

(a) Mach number

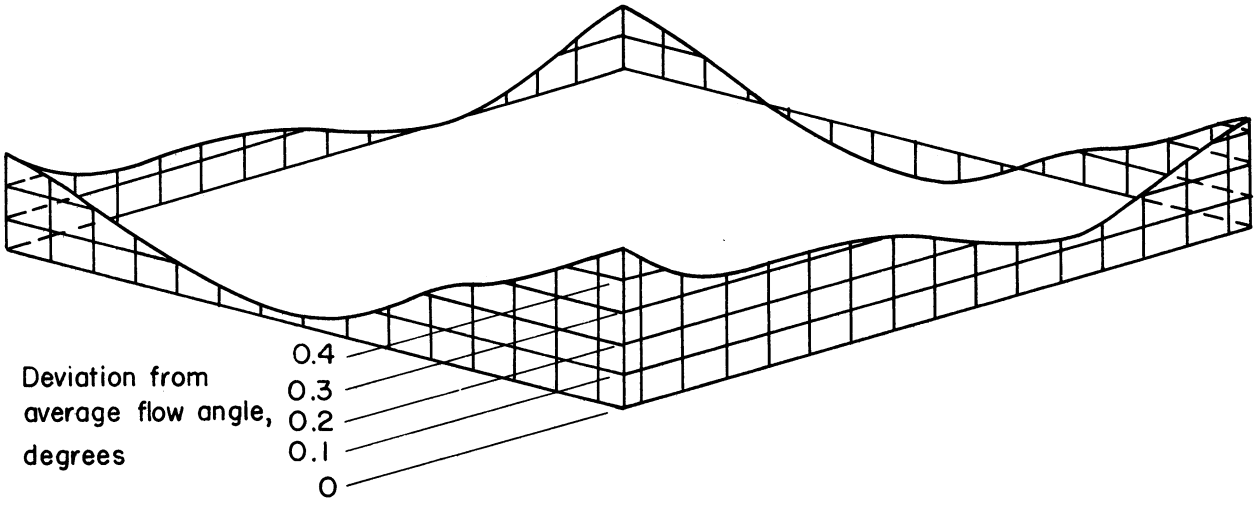

(b) Flow angle

Fig. 3.22. Mach number and flow-angle variation along test-rhombus perimeter. M = 3.84.

Mach number or flow angle from the average, within a 4-inch-high test rhombus centered at the nozzle exit (end of curved part of upper contour). For this rhombus the horizontally projected throat-to-test-rhombus distance varies between 6.4 and 8.8 times the rhombus height of 4 inches for Mach numbers from about 1.5 to 4.0.

As shown in Fig. 3.13, the Mach number deviation from the average within the test rhombus is less than $\pm$ 0.9% for each Mach number tested in the range M = 1.3 to 4.0. The flow angle deviation is less than $\pm$ 0.5°. The highest Mach number obtained, due to mechanical limitations in the lower block traversing mechanism, was 3.84, but the trend of the data suggests that a considerable increase in Mach number might be realized before the above deviation limits would be exceeded.

Figs. 3.14 to 3.22 present details of the flow along the edges of the test rhombus at nine Mach numbers from 1.27 to 3.84. It should be noted that the Mach number (or flow angle) at any point within the test rhombus can be easily determined by moving any of the edge curves (in the appropriate diagram) parallel to itself to the position in question, keeping the ends of the curve on the adjacent edge curves. This process is illustrated in Fig. 3.18 where the Mach number deviation at point D is determined.

The change of average Mach number in the test rhombus with lower block axial position is presented in Fig. 3.23 together with the theoretical variation based on the measured throat-to-test-section area ratios. The slight change in slope of the theoretical curve at M = 1.44 is caused by a shift in the geometric throat position at this Mach number.

Only data from the pitot rake tests at Mach numbers from 1.6 to 3.8 appear in Fig. 3.23. The tests at Mach numbers 1.27 to 1.51 gave only the relative variation of Mach number within the test rhombus. For these lower Mach numbers, the absolute Mach number level was determined from Fig. 3.23.

3.3.2 Reynolds' Number Effect.—The data from the tests at stagnation pressures of from 2 to 6 atmospheres are presented in Fig 3.24. Comparison of the plotted points with the solid curve, representing the atmospheric pressure results, shows that the difference in Mach number distribution in the test section, due to a sixfold increase in Reynolds' number, is within the measuring accuracy.

The effect of Reynolds' number change on the average Mach number within the test rhombus is shown in Fig. 3.25. Also shown on this figure is an extrapolation to zero boundary-layer thickness by means of one-dimensional theory. (According to the Tucker method, the boundary-layer thickness is proportional to the parameter $(1/Re)^{1/7}$).

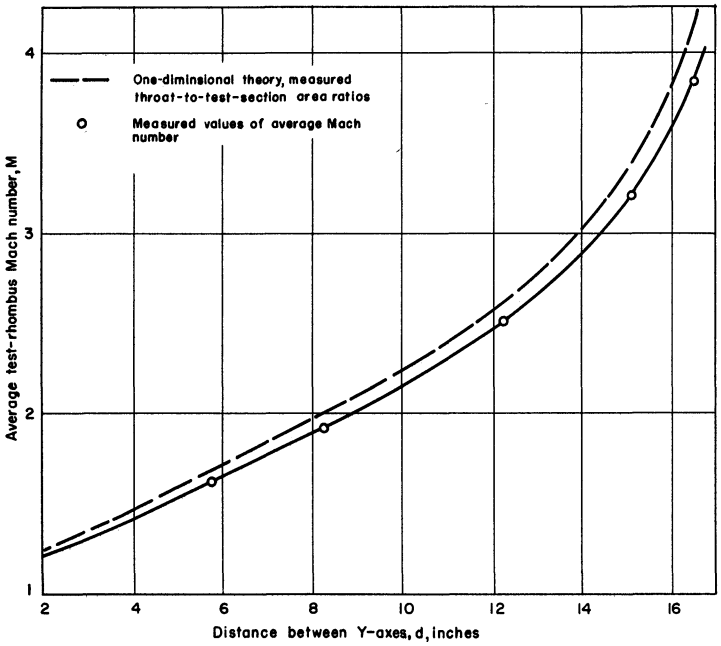

Fig. 3.23. Relationship between lower-block axial setting and average test-rhombus Mach number.

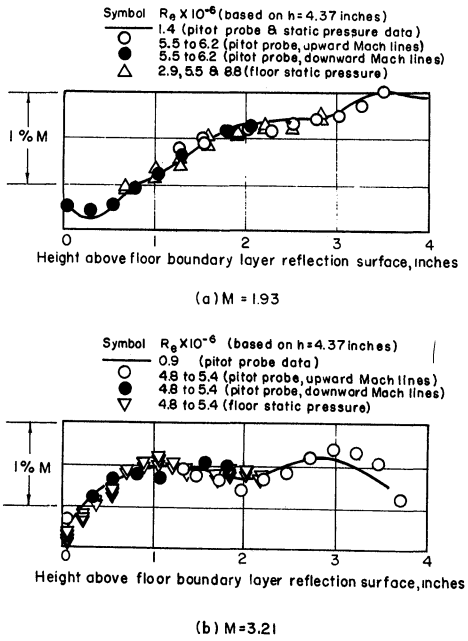

Fig. 3.24. Mach number variation along exit Mach line at higher Reynolds' numbers.

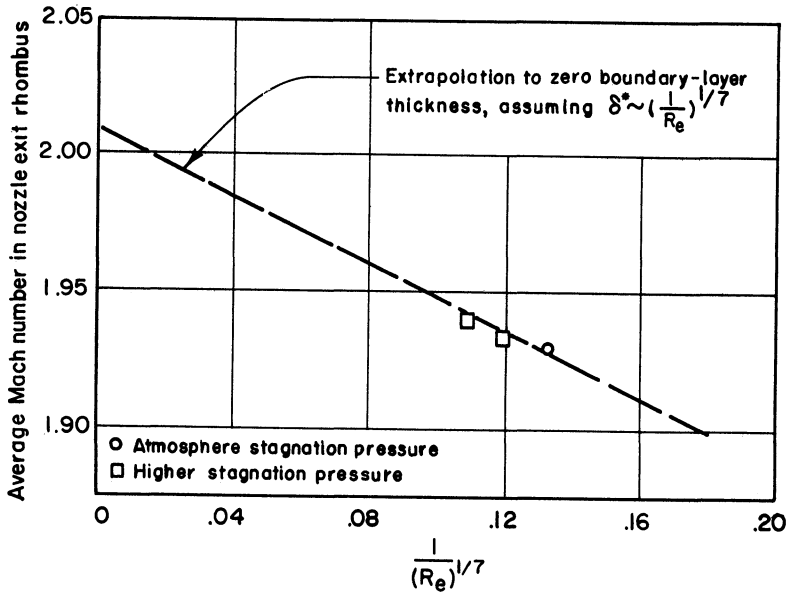

Fig. 3.25. Effect of Reynolds' number on average test-rhombus Mach number.

SECTION 4

DISCUSSION

4.1 RECOMMENDED CONTOURS

4.1.1 Nozzle Coordinates.—The final faired coordinates listed in Table 2.2 are recommended for use in wind tunnels designed for the Reynolds' number range of the present tests. These recommended contours differ from the tested contours by amounts up to 0.004 inches, but the difference is such that unnecessary waviness between jacks in the actual nozzle is eliminated in the final faired coordinates. It is therefore believed that the coordinates of Table 2.2 should give flow uniformity as good as, or better than, that of the actual nozzle (Fig. 3.13).

4.1.2 Contour Tolerances.—The analysis of Appendix E shows that flow-angle errors greater than $\pm \Delta\alpha$ degrees due to contour defects will be avoided if the coordinates of the nozzle are accurate to within $\pm 0.02\Delta\alpha$ inches, and if certain tolerances on short wavelength waviness are met. These waviness tolerances can be stated in terms of the reading of a curvature gage of the type shown in Fig. 2.4. Such a gage reads a value G in inches given in terms of the coordinates as

$$G = \frac{\Delta^2 y}{\left[1 + \left(\frac{\Delta y}{\Delta x}\right)^2\right]^{3/2}}$$

where Δx equals the distance in inches between the center contact and each of the two outer contacts (the gage length, lg), Δy is the change in y, in inches, associated with Δx, and $\Delta^2 y$ is the difference between the Δy's of the two adjacent Δx intervals spanned by the gage (second difference). For a given gage length and nozzle size, the correct values of G may be computed from the equation and the coordinates of Table 2.2. As an example, values of G that are consistent with the coordinates of Table 2.2 for the lower contour of a nozzle having a value of height between coordinate axes, h, of 4.37 inches are plotted in Fig. 4.1, for a 1/4-inch curvature gage (lg = 1/4 inch), and for a 1-inch gage.

If the readings of a 1-inch curvature gage do not depart from the correct values computed from the above equation by more than $\pm 0.014\ \Delta\alpha$ inches, then the test-section flow should be free of flow-angle errors greater than $\pm \Delta\alpha$ degrees due to contour defects having wavelengths greater than 1.55 inches. If, in addition, the readings of a 1/4-inch curvature gage agree with the correct values to within $\pm 0.004\ \Delta\alpha$ inches, then flow-angle errors due to all defects having wavelengths greater than 0.4 inches will be less than $\pm \Delta\alpha$ degrees.

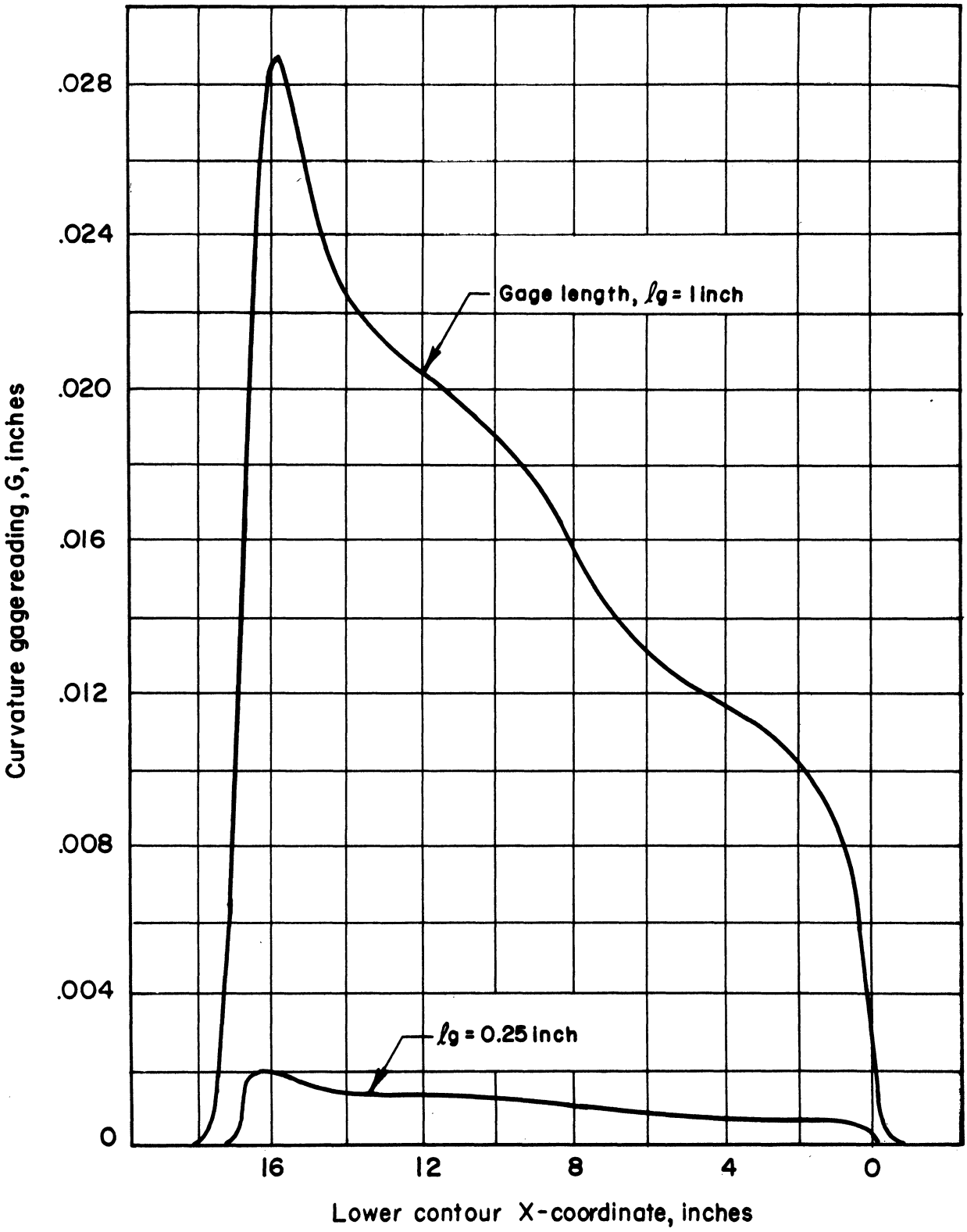

Fig. 4.1. Curvature gage readings of lower contour, consistent with the faired final coordinates for a nozzle having h = 4.37 inches.

4.1.3 Scale Effects.—The faired contours given in Table 2.2 should produce satisfactory flow for nozzle sizes and stagnation conditions represented by $.0228 < h\ p_o/T_o^{1.26} < .160$, where p_o is the stagnation pressure in psia, T_o is the stagnation temperature in degrees Rankine, and h is the vertical distance in inches between coordinate origins of the two blocks (h = 4.37 inches for the present nozzle). At any given Mach number the Reynolds' number is approximately proportional to the parameter $h\ p_o/T_o^{1.26}$ (assuming the viscosity $\mu = \mu_o(T/T_o)^{.76}$). For the above range of this parameter, the corresponding Reynolds' numbers based on h are Re = 1.68 to 11.8 x 10^6 at M = 1.27 and Re = .55 to 3.86 x 10^6 at M = 3.84.

For combinations of stagnation conditions and nozzle size outside the above range, it may be desirable to alter the contours of Table 2.2 to compensate for the change in boundary-layer thickness. One approximate way of doing this would be to reduce the lower block y-values and increase those of the upper block by the difference between boundary-layer corrections computed at the old and new Reynolds' numbers, for some arbitrary Mach number.

4.2 FURTHER POSSIBLE IMPROVEMENTS

From the trend of flow uniformity at the upper end of the Mach number range, as shown in Fig. 3.13, it appears that the present contours would give satisfactory flow at Mach numbers somewhat greater than 4.0. With some further refinement of the contours it would seem possible for a nozzle of this type to reach the threshold of the hypersonic regime.

Improvements in the performance of diffusers used with sliding-block nozzles may also be possible. Some tests with an adjustable diffuser (Appendix F) in combination with the present nozzle resulted in overall pressure ratios of about the same magnitudes as those obtained with fixed geometry diffusers on symmetrical nozzles.

4.3 FLOW MECHANISM

An attempt is made to arrive at a simple picture of the flow mechanism in a curved nozzle from an analysis of the experimental data and the contour corrections which gave the most uniform flow over the Mach number range investigated.

Most of the usual causes for nonuniformities in a supersonic nozzle have been minimized in the construction of this model. There are no junctures in the tunnel walls in the supersonic region, and the contoured surfaces are extremely smooth and free from local manufacturing defects; the deflections under airloads were held to a negligible amount; and the inflatable seals

assured the absence of leakage. Humidity effects were also absent due to the low dew points used.

The nonuniformities in the flow with theoretical contours may therefore be an indication of the interactions between viscous and non-viscous flow regimes, of secondary boundary-layer flows due to curvature, and of other effects which cannot be predicted by available theory. An explanation of these effects is obviously involved and difficult and would have required detailed probing of the boundary layers on all four walls of the nozzle. This was not possible under the present program and one can only list all pertinent experimental results and attempt to deduce a likely flow mechanism which will best fit the results.

From an evaluation of all available test data, the following general statements can be made:

a) A compression region originates or reflects from the upper contour just upstream of the nozzle exit Mach line.

b) An expansion region originates or reflects from the lower contour just downstream of the compression region described above.

c) The location of this pair of compressions and expansions with respect to the exit Mach line is independent of the Mach number and Reynolds' number within the range of the tests.

d) The axial length of the compression region increases with increasing Mach number. The overall strength remains approximately constant at the higher Mach numbers and decreases with lower Mach numbers.

e) A downward flow exists in the sidewall boundary layer, which appears to be most pronounced near the center of the simple wave flow region of the nozzle.

f) A lateral flow towards the vertical plane of symmetry exists on the lower nozzle, which increases as the nozzle exit is approached.

g) The application of boundary-layer displacement-thickness corrections to the theoretical nozzle contours reduced the strength of the compression disturbances somewhat.

h) Reduction of the strength of the compression disturbances to an acceptable value was accomplished in the final contours by introducing a local slope change in the upper contour just upstream of the nozzle exit Mach line.

The following crude flow mechanism is believed to be consistent with the results:

The curvature of the flow in the nozzle gives rise to a centripetal pressure gradient. This pressure gradient extends into the sidewall boundary layers and causes a boundary-layer cross-flow toward the lower contour which, in turn, leads to a cross flow in the floor boundary layer toward its plane of symmetry. The result is a gradual secondary thickening of the floor boundary layer beyond its normal two-dimensional growth. The cross-flow pattern, observed with the china clay technique, indicates that the rate of secondary thickening of the floor boundary layer should reach a maximum just upstream of the exit Mach line. As soon as the flow in the nozzle is straight, however, the cross flow effects begin to diminish and the secondary thickening of the floor boundary layer gradually approaches zero.

The general location of this secondary thickening of the floor boundary layer will be the same for all Mach numbers. As the Mach number increases, however, the increased boundary-layer thicknesses on the sides will lead to a larger cross flow, which in turn will spread the secondary thickening on the floor over a larger region.

The mechanism described above appears to be the most likely cause for the experimental results noted. The local compression region observed is then caused by the increasing slope portion of the secondary boundary-layer thickening. An expansion region follows this compression; it starts at the maximum slope point of the secondary thickening and extends over the decreasing slope region until the secondary thickening disappears. The expansion is spread over a greater distance so that the local strength of its waves which travel into the test section is less pronounced and well within the acceptable level of disturbances in the flow.

The compression occurs just upstream of the exit Mach line, is transmitted parallel to it to the top surface, and then reflected into the test section. Changing the slope of the upper contour in the region of reflection of this compression resulted in an appreciable reduction of this disturbance.

SECTION 5

CONCLUSIONS

1. A sliding-block variable Mach number wind-tunnel nozzle for the Mach number range 1.3 to 4.0 has been developed, by means of iterative characteristic theory with experimental corrections. Calibration of the flow in this nozzle has revealed the following:

a) The Mach number deviation from the average within a test rhombus is less than $\pm$ 0.9% throughout the Mach number range 1.3 to 4.0.

b) In this range the flow angle deviation from the average within a test rhombus is less than $\pm$ 0.5°.

c) The horizontally projected throat-to-test rhombus center distance is 8.8 times the test rhombus height at the highest Mach number.

d) A six-fold increase in Reynolds' number has negligible effect on the flow uniformity.

e) The overall pressure ratios required to run the nozzle with an adjustable diffuser are about the same as those required by symmetrical nozzles with fixed diffusers.

2. An economical, general purpose, variable Mach number supersonic nozzle can be designed from the material of this report provided the length of the nozzle can be accommodated.

3. The nozzle appears suitable for the simulation of time-variable Mach number conditions.

4. Additional work on this nozzle could lead to an extension of the Mach number range into the hypersonic and transonic regimes.

SECTION 6

REFERENCES

1. Allen, H. Julian. The Asymmetric Adjustable Supersonic Nozzle for Wind Tunnel Application. NACA TN 2919. March 1953.

2. Syvertson, Clarence A. and Savin, Raymond C. The Design of Variable Mach Number Asymmetric Supersonic Nozzles by Two Procedures Employing Inclined and Curved Sonic Lines. NACA TN 2922. March 1953.

3. Burbank, Paige B. and Byrne, Robert W. The Aerodynamic Design and Calibration of an Asymmetric Variable Mach Number Nozzle with a Sliding Block for the Mach Number Range, 1.27 to 2.75. NACA TN 2921. April 1953.

4. Murphy, J. S. and Buning, H. Theory and Design of a Variable Mach Number Corner Nozzle. University of Michigan. WTM 221. April-December 1951.

5. Liepman, H. P. An Analytic Design Method for a Two-Dimensional Asymmetric Curved Nozzle. University of Michigan. June 1953.

6. Liepman, H. P., Murphy, J. S. and Nourse, J. H. A Physical Description of a Variable-Mach-Number 4-by 4-Inch Pilot Corner Nozzle. University of Michigan. WTM 246. December 1953.

7. Fashbaugh, R. H. Supersonic Wind Tunnel 8-Inch Schlieren System Operation and Maintenance Manual. University of Michigan. WTM 243. May 1954.

8. Haefeli, Rudolph C. Use of Fences to Increase Uniformity of Boundary Layer on Side Walls of Supersonic Wind Tunnels. NACA RM E52E19. July 1952.

9. Tucker, Maurice. Approximate Calculation of Turbulent Boundary Layer Development in Compressible Flow. NACA TN 2337. April 1951.

10. Gieseler, L. P. Continuous Recording of Pressures for Supersonic Wind Tunnel Calibration. NAVORD Report No. 2744. 1953.

SECTION 7

APPENDICES

APPENDIX A

DESIGN DETAILS OF FLEXIBLE PLATE AND JACKS

A.1 INTRODUCTION

The aerodynamic requirements for the nozzle are given in Reference 4. Reference 6 gives a brief description of the experimental equipment which was fabricated for the evaluation of this type of supersonic nozzle. In addition to these references, a more specific discussion of the design and performance of the flexible plate portion of the corner nozzle is given here.

A.2 THE DESIGN PROBLEM

The following major considerations were involved in the design of the flexible plate:

(a) The flexible portion of the nozzle was to be made from a smoothly machined flat plate by bending it to the desired contours and holding it there with jacks, which had to be capable of introducing specified small contour perturbations. The perturbation requirement was specified to allow for contour corrections due to viscous effects, deviations from two-dimensional flow, and shortcomings of theoretical predictions.

(b) The position and number of jacks had to be chosen so that the flexible plates could be controlled to the specified contours and contour perturbations within $\pm$ 0.002 inches.

(c) The maximum stresses in the plates due to initial bending, airloads, temperature effects, and thrustloads were not to exceed about one-half of the yield point of the material.

A.3 THE DESIGN PROCEDURE

The design and fabrication of the corner nozzle, including the flexible plates, was subcontracted to the Wind Tunnel Instrument Company of Boston, Massachusetts. The specifications for this work are given in Appendix A of Reference 6. The analysis of the problem by the subcontractor is contained in

a report by H. L. Alden, entitled "Flexible Plate Design for the University of Michigan 4" x 4" Supersonic Wind Tunnel Test Section," dated November 1952. This report is on file at the offices of the Wind Tunnel Instrument Company.

The following is a brief outline of the design procedure, which has led to a highly satisfactory and reliable flexible-plate nozzle.

(a) The jack spacing and plate thickness were approximately determined so that the deflections under airloads were within specified limits.

(b) The jack spacing was also approximately determined by considering the bending requirements of the plate; the specified curvature of the contour was approximated by straight lines between jacks to provide a M/EI-diagram as first approximation.

(c) The approximations of steps (a) and (b) lead to a nominal plate thickness of 1/4 inch.

(d) The yield stress safety factor of two indicated that the thickness of the lower plate had to be decreased in the highly curved (upstream) region.

(e) The jack spacing was now finalized by assuming a constant thickness plate, selecting tentative jack stations, and fitting between them curves whose bending moment (and hence second derivative) are linear between stations. This is equivalent to an ordinate curve which is a cubic in x and matches the contours specified. Each span will have a different cubic while, across the jacks, each cubic must be continuous up through the second derivative; the third derivative is discontinuous, corresponding to jumps in the shearing force.

A trial-and-error procedure was carried out with a cubic of the form $y = A+Bx + (C/2)x^2 + (D/6)x^3$ for each span. The constants A, B, and C are determined by the end conditions of one end of each span, while D is determined by conditions at the other end of the span (whose length is not yet known) such that ordinate, slope, and curvature are consistent and proper. For the first span in each plate, different values of D and x must be tried until all conditions are met. Subsequent spans require only trials on D. If no satisfactory match could be obtained, the constants of the neighboring spans had to be considered and even readjusted.

In this manner the jack stations were determined for both flexible plates.

(f) A similar trial-and-error procedure was used to determine the jack adjustments needed to satisfy the requirements of the perturbation bending of the plates.

(g) The constants of the cubics of the final design curves are related to bending moment (M_b), shear (V), and stress (S) in the plate, through the following obvious relations:

$$M_b = \frac{EI}{(1 - \nu^2)} C \qquad (A\text{-}1)$$

$$V = \frac{EI}{(1 - \nu^2)} D \qquad (A\text{-}2)$$

$$S = \frac{Et}{2(1 - \nu^2)} \frac{d^2y}{dx^2} \qquad (A\text{-}3)$$

where ν = Poisson's Ratio
t = plate thickness
I = moment of inertia of plate
E = Young's modulus

(h) Finally, the plate thickness in the three upstream spans of the lower plate had to be reduced to bring the stress level to an acceptable value. This was done by retaining the original design curve as represented by the constants A, B, C, and D in the three spans and by readjusting the moments, reactions, and thickness (or moment of inertia I) in such a way that all compensate each other as far as deflections are concerned, while, at the same time, reducing the stress in these sections to the desired level. This procedure led to a nearly linear variation in thickness, which was very fortunate from a manufacturing standpoint but was due to circumstances, not to special design practice. The thickness variation of the lower plate is shown in Fig. A. 1. The upper plate has a constant thickness of 1/4 inch.

(i) Deflections due to airloads and shears were checked and found to be within the specified limits.

The plate stresses due to temperature differentials and thrust loads were checked and found to be negligible.

The major results of the flexible plate design are given in Figs. A.1 and A.2. Shown are the geometry of the plates with their jack spacing, the curvature distribution as designed and as specified, the bending-to-contour stresses calculated and measured with strain gages during the initial assembly of the plates, and the deviations from specified ordinates as measured by a height gage after initial assembly.

The flexible plates were made from Vulcan Hecla Steel, SAE 6150, heat-treated to a yield point of about 140,000 psi. All aerodynamic surfaces were ground.

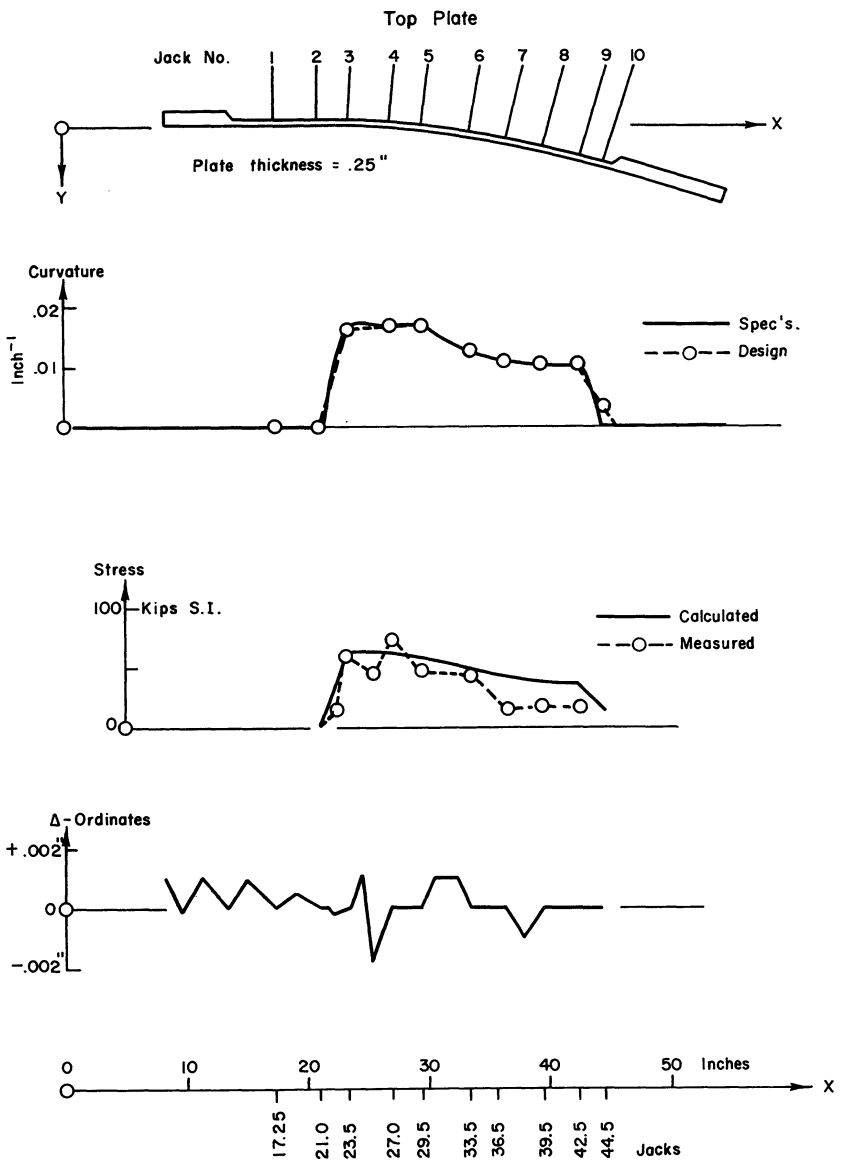

Fig. A.1. Structural properties of lower contour flexible plate.

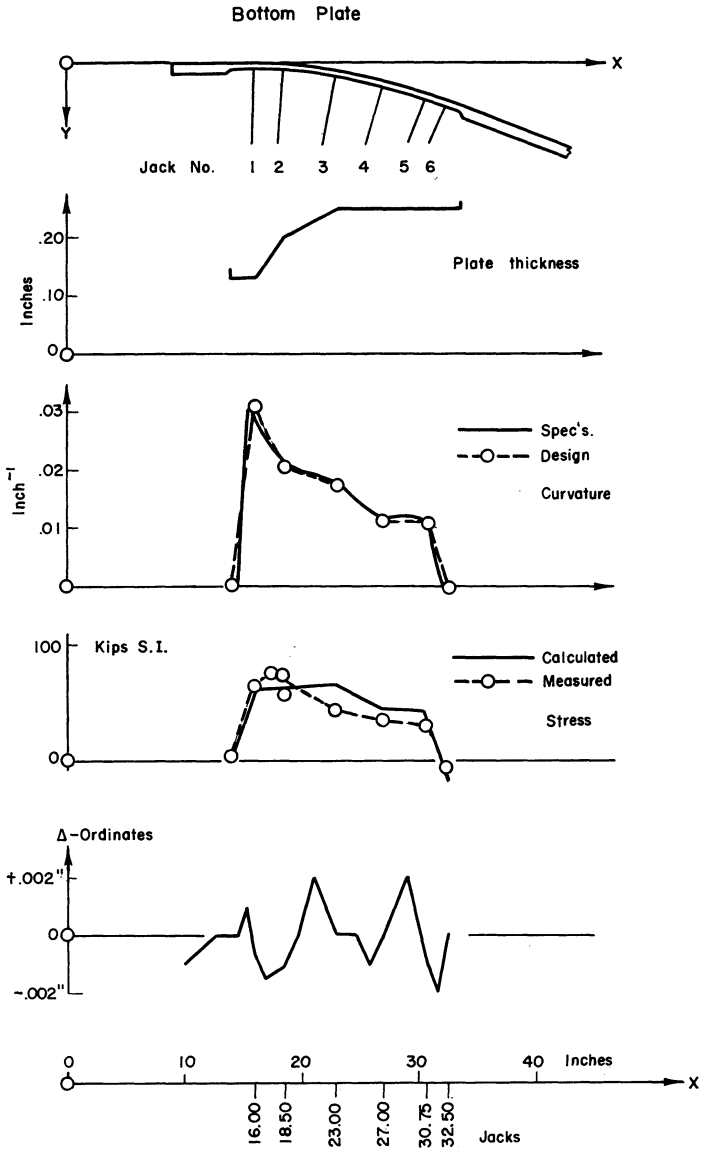

Fig. A.2. Structural properties of upper contour flexible plate.

A.4 JACK ATTACHMENT DESIGN

The design of the flexible plate was carried out under the assumption that the jack attachments introduce only forces which are normal to the plate. This is, of course, highly idealized, and one must assume that some moment reaction is set up at a jack attachment due to the combined loadings of bending, air loads, temperature differential, perturbation bending, and manufacturing eccentricities. Thus, the question arises as to how much of a stray moment can be tolerated at the jack points. To gain an approximate answer to this question, a simplified section of the flexible plate with three jack points was analyzed, as sketched in Fig. A.3. A concentrated jack moment at the center support was calculated, assuming negligible support moments at the end support, and a maximum deflection of 0.001 inch in the spans. This moment was found to be 300 in.-lb. On the basis of this calculation, a maximum allowable stray moment of 100 in.-lb was conservatively specified.

The design of the jack attachment was conditioned by the decision to employ a small tang, machined integrally with the plate stock, to avoid local changes in material properties and nonuniformities in the plate, and to relieve moments through flexure of the tang. To reduce as much as possible the need for bending of the tang, a jack support system was selected which has a pin joint at its lower end. A schematic of the final configuration is shown in Fig. A.4 and the detail of the tang in Fig. A.5.

The calculated performance of this design is well within the desired limits under extreme conditions of loading; for a typical jack with a jack length (l_j) of 4 inches, a tang length (l) of 1/8 inch, tang thickness (t) of 1/32 inch, and tang width of 4 inches, the support moments and stresses in the tang are as follows:

Loading	Support Moment in.-lb	Tang Stress psi
(1) Temperature differential (.01-in. plate-wise motion)	5.6	8,600
(2) Jack load of 1500 lb	.3	12,000
(3) Perturbation bending	22.1	34,000
Total of loads (1) + (2) + (3)	28.0	54,600

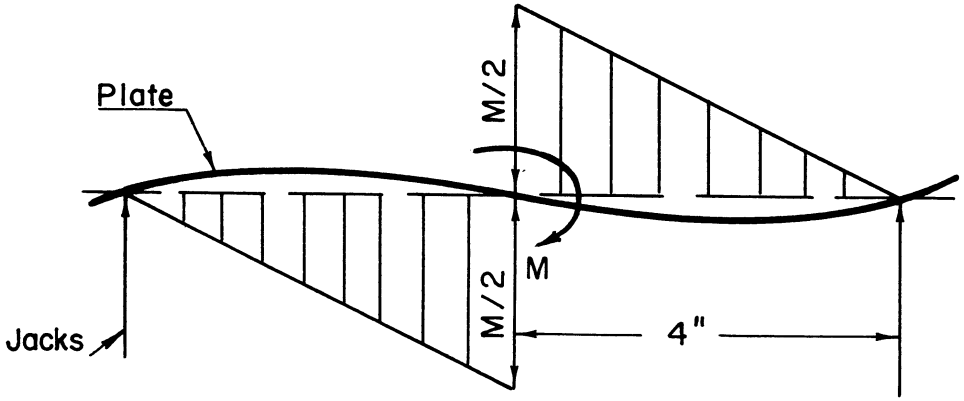

Fig. A.3. Effect of jack moment on flexible plate contour.

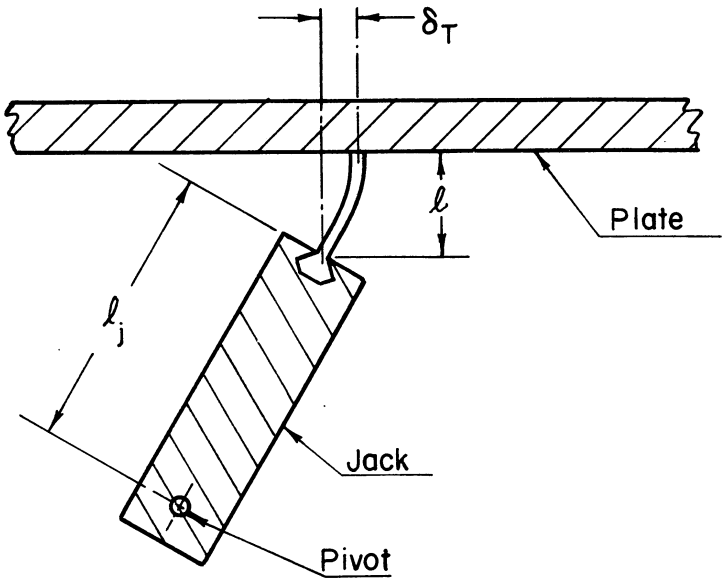

Fig. A.4. Geometry of jack attachment.

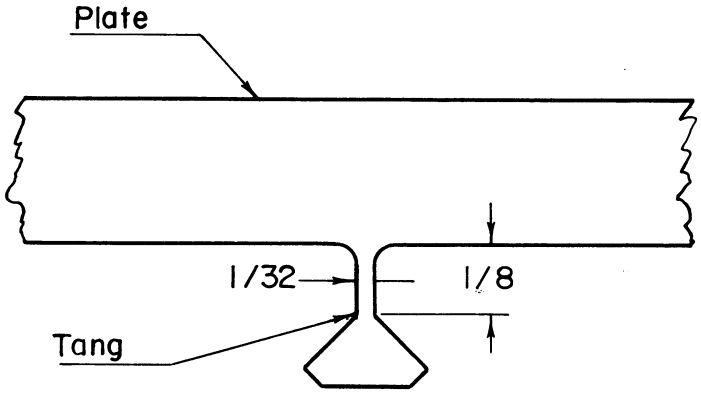

Fig. A.5. Detail of jack attachment tang.

The actual performance of the jack-and-plate assembly under severe operating conditions has indicated no noticeable deflection at the supports, nor has there been any structural failure.

APPENDIX B

NOZZLE SEALS

Atmospheric air was prevented from leaking into the aerodynamic channel by inflatable seals made of Emson black rubber tubing with 1/8-inch inside diameter and 1/32-inch wall thickness placed in strategically located grooves. Proper functioning of these seals was tested by evacuating the tunnel to about one inch of mercury absolute pressure, and increasing the seal pressure until the noise caused by leakage stopped. The seal pressure necessary for effective sealing was found to be 30 psi for the nozzle seals, and 60 psi for the diffuser, due to the existence of somewhat larger grooves in the diffuser.

Considerable difficulty was experienced with seal longevity. The seals failed twice by being pinched and punctured in the narrow gap between the lower block and the side walls, during translation of the lower block. It was finally found that the seal life could be greatly increased by lubrication with a silicone type of vacuum grease.

APPENDIX C

MOVING PROBE TECHNIQUE

Early in the flow evaluation tests with the original contours, the moving probe technique was tried as a means of obtaining a maximum of data per run. This technique consisted of recording pressures on a pitot probe rake which was traversed axially or vertically during a run. The pressures were sensed by pressure capsules containing Schaevitz transformers, and recorded on a Sanborn recorder. (See Reference 10 for a description of a similar technique.)

Tests with the moving probe showed no steep pressure gradients such as would be caused by shock waves. This result is also confirmed by the lack of visible disturbances in schlieren pictures. The absence of shock waves is attributed to the fact that there are no junctures in the supersonic part of the nozzle, and that the contours have a minimum of short-length waviness.

After these traveling probe tests had been begun, it was realized that pressure data taken along the horizontal centerline of a tunnel do not reveal the characteristics of the flow unless the flow is symmetrical about the horizontal center plane. In an asymmetrical two-dimensional tunnel the most significant data is that taken along the Mach lines or along the floor or ceiling (see Appendix D). The traveling probe method was therefore supplanted for the rest of the tests by either point-by-point probing along Mach lines or floor static-pressure measurements, since the probe mechanism was not easily traversed along Mach lines.

APPENDIX D

ANALYSIS OF TWO DIMENSIONAL TEST SECTION FLOW BY LINEAR THEORY

In calibrating a supersonic wind tunnel, it is desirable to obtain information about the flow at every point of the test section without having to make an excessive number of measurements. One way of reducing the number of measurements required would be to use the method of characteristics to determine the flow properties at any point in the flow from measurements made along a single line. However, the flow in a wind-tunnel test section is so nearly uniform that the method of characteristics may be linearized with little loss of accuracy. The linearized theory is used below to derive a rapid method of determining the test-section flow properties from a limited number of measurements.

The basic simplification introduced by the linear theory is that the compression and expansion waves producing the small disturbances from uniformity are everywhere straight and inclined to the axis of the channel at the same angle, which is the Mach angle corresponding to the average Mach number of the flow. This assumption will be quite close to the truth in a wind-tunnel test section, where the Mach number variation is usually of the order of $\pm$ 1%. (A 1% change in Mach number would give less than 1° change in the direction of a Mach line at M = 1.4, and much less at higher Mach numbers.) It will also be assumed that the flow is two-dimensional and inviscid, and that the channel has straight walls, not necessarily parallel.

Suppose the direction of the flow at every point on a Mach line ab is known (see Sketch 1). Any deviation of flow direction from that which exists at a can be considered to result from weak expansion or compression waves crossing ab. Then, with the assumption that all these weak waves run at the average Mach angle, and supposing the channel to have straight walls, the flow direction at any other point in the channel can be easily determined.

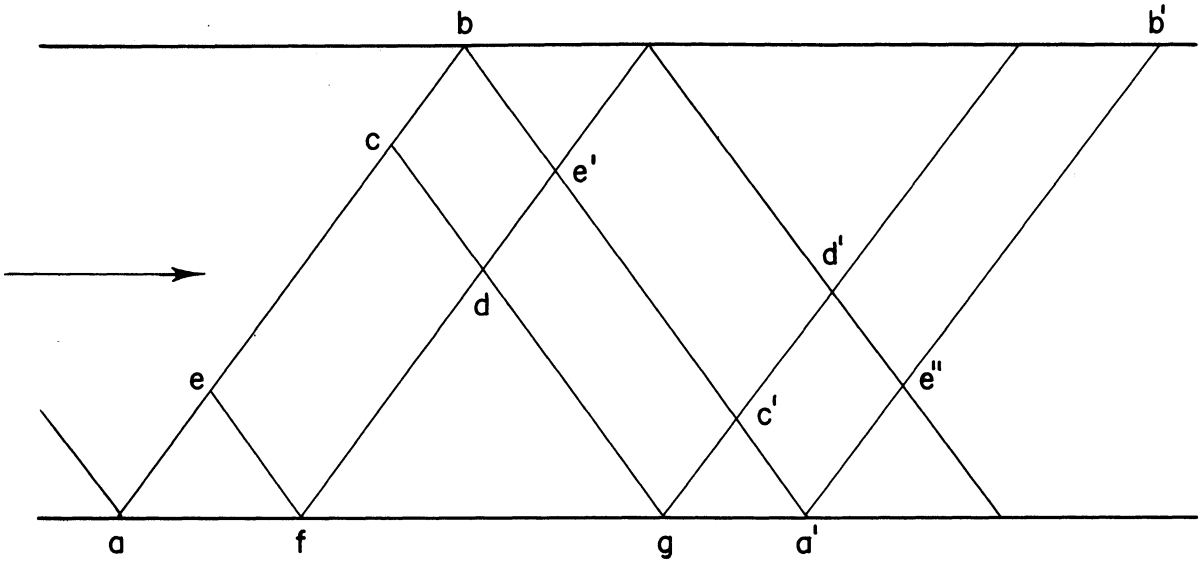

Sketch 1

Referring to Sketch 1, it can be seen that the flow angle θ (the angle between a fixed reference line and the flow direction) at any point d between Mach line ab and its reflection ba' is

$$\theta_d = \theta_f + (\theta_c - \theta_e)$$

since the same Mach waves cross ec as cross fd. Now $\theta_a = \theta_f$ since at the wall the flow must be in the direction of the wall. Thus

$$\theta_d = \theta_a + \theta_c - \theta_e \qquad \text{(D-1)}$$

Similarly, for a point d' between the first reflection ba' and the second reflection a'b'

$$\begin{aligned} \theta_{d'} &= \theta_g + (\theta_b - \theta_c) + (\theta_{e''} - \theta_{a'}) \\ &= \theta_a + (\theta_b - \theta_c) + (\theta_e - \theta_a) \\ &= \theta_b + \theta_e - \theta_c \qquad \text{(D-2)} \end{aligned}$$

The flow angles repeat after the second reflection. Thus the flow direction at any point in the flow may be easily found from the flow angle distribution along a Mach line.

If only small changes in Mach number are considered, the Mach number variation along a Mach line can be taken proportional to the flow angle variation, in accordance with linear theory. Thus, with reasoning similar to that used above, it is seen that the Mach number at any point d is

$$M_d = M_c + (M_f - M_e)$$

$$= M_c + (M_e - M_a)$$

$$= M_a + (M_c - M_a) + (M_e - M_a) \qquad (D\text{-}3)$$

A similar formula holds for a point d' at the intersection of any number of reflections of the Mach lines through c and e.

The Mach number distribution along the floor or ceiling of the channel is found from the above formula to be

$$M_f = M_a + 2(M_e - M_a) \qquad (D\text{-}4)$$

This formula can be rearranged to give the variation of M along a Mach line once the wall distribution is known. Thus the test-section flow can be completely determined from static pressure distribution along a length of floor or ceiling equal to the distance ab' if the stagnation pressure is known.

It should be noted that the variation of Mach number along a Mach line is the same along every reflection of that Mach line. The Mach number at any point e' of ba' (Sketch 1) will differ from that at b by the same amount as the corresponding point e of ab differs from a. Thus the wavelength of the Mach number variation along a Mach line is the distance between channel walls along a Mach line. If the walls diverge or converge slightly, the Mach number at any point of ba' will differ by a constant from that of the corresponding point of ab.

The maximum variation in Mach number within a test rhombus, which is of interest in wind-tunnel calibration, can be determined directly from the Mach number variation along a Mach line. If the rhombus is bounded on one side by the known Mach line (ab in Sketch 2), then the most upstream point, p, of

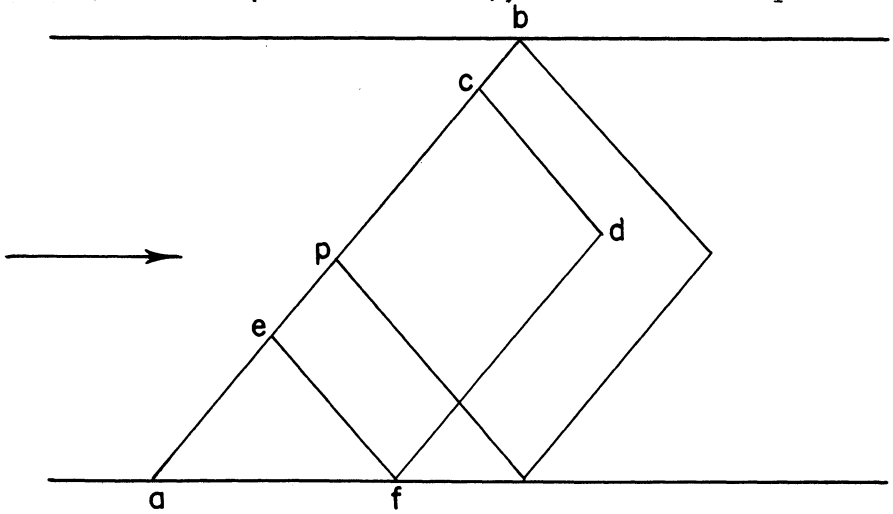

Sketch 2

the rhombus divides ab into two halves. Equation (D-3) can then be expanded to give the Mach number at any point d in the rhombus in terms of the Mach number variation in these two halves, ap and pb. Thus,

$$M_d = M_p + (M_c - M_p) + (M_e - M_a) \tag{D-5}$$

The highest Mach number in the rhombus will be

$$M_{max} = M_p + (M_{max_{pb}} - M_p) + (M_{max_{ap}} - M_a) \tag{D-6}$$

where $M_{max_{ap}}$ and $M_{max_{pb}}$ are the maximum Mach numbers in the first and second halves of ab, respectively. Similarly,

$$M_{min} = M_p + (M_{min_{pb}} - M_p) + (M_{min_{ap}} - M_a) \tag{D-7}$$

The extreme variation of Mach number within the rhombus can be written by combining (D-6) and (D-7), as

$$\begin{aligned} \Delta M &= M_{max} - M_{min} \\ &= (M_{max} - M_{min})_{ap} + (M_{max} - M_{min})_{pb} \end{aligned} \tag{D-8}$$

Thus the extreme Mach number variation ΔM in the rhombus is the sum of the extreme variations in the two halves of the Mach number distribution along a Mach line. This value of ΔM must be greater than one, but less than two, times the Mach number variation along a Mach line.

If the Mach number distribution is not known along a line coinciding with one side of the desired test rhombus, it can be easily found, as shown in Sketch 3, where ab is the known Mach line and fh is a line along the desired

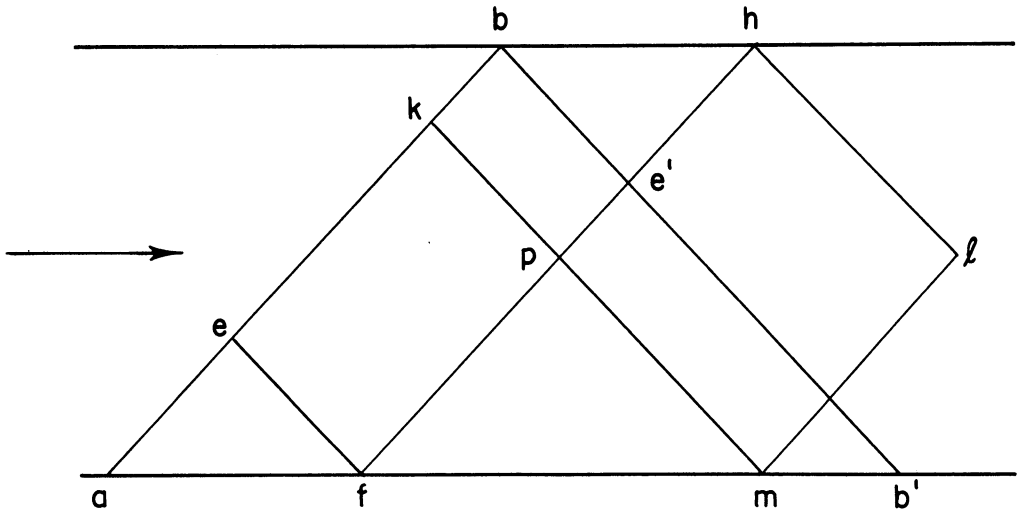

Sketch 3

rhombus. The variation in Mach number along fe' will be the same as that along eb since the same expansion or compression waves cross these lines. The variation along e'h will be the same as that along be' or ae, for the same reason.

A diagram showing how the magnitude of ΔM varies as the rhombus location is shifted along the tunnel axis can be easily constructed. For this purpose the extreme Mach number variation ΔM_{phlm} in the general rhombus phlm of Sketch 3 can be written, using equation (D-8), as

$$\Delta M_{phlm} = M_{max_{fp}} - M_{min_{fp}} + M_{max_{ph}} - M_{min_{ph}}$$

$$= M_{max_{ek}} - M_{min_{ek}} + M_{max_{kbe'}} - M_{min_{kbe'}}$$

(Note that the variation of Mach number along ph is the same as that along kbe', since the same Mach waves cross corresponding points of both lines. The Mach numbers along be' equal those at corresponding points of ae, with the addition of the constant $(M_b - M_a)$.) This can be expanded to

$$\Delta M_{phlm} = (M_b - M_a) + (M_e - M_{min_{ek}}) + (M_k - M_{min_{kbe'}}) + (M_{max_{ek}} - M_k) + (M_{max_{kbe'}} - M_e - M_b + M_a)$$

$$= (M_b - M_a) + (M_e - M_{min_{ek}}) + (M_k - M_{min_{kbe'}}) + (M_{max_{ek}} - M_k) + (M_{max_{kbe'}} - M_{e'}) \qquad \text{(D-9)}$$

In Sketch 3 and equation (D-9) the points a and b are fixed at the ends of the known Mach line. The other points move with respect to a and b as the rhombus location is varied. Thus, the first term on the right side of equation (D-9) is a constant, and the other four are functions of rhombus position.

A convenient method for evaluating the variable terms in equation (D-9) is illustrated in Sketch 4. The heavy line in part (a) of this figure represents a typical distribution of Mach number along a Mach line from floor to ceiling (ab in Sketch 3) and its reflection to b'. The shaded areas below the heavy curve in Sketch 4(a) are generated by sliding the curve to the left a distance equal to half of ab; those above, by sliding to the right. It is seen that the Mach number difference between the heavy curve at point e and the bottom of the shaded area at that point is equal to $(M_e - M_{min_{ek}})$. Similarly, the last three terms of equation (D-9) are represented in Sketch 4(a) by the height of the shaded area below the curve at k, above the curve at k, and above the curve at e', respectively. Note that the height of shaded area above the curve at e' is the same as that at e, so that the sum of the four variable terms of equation (D-9) is represented by the sum of the Mach number differences between top and bottom of the shaded areas at e and k. Thus, for

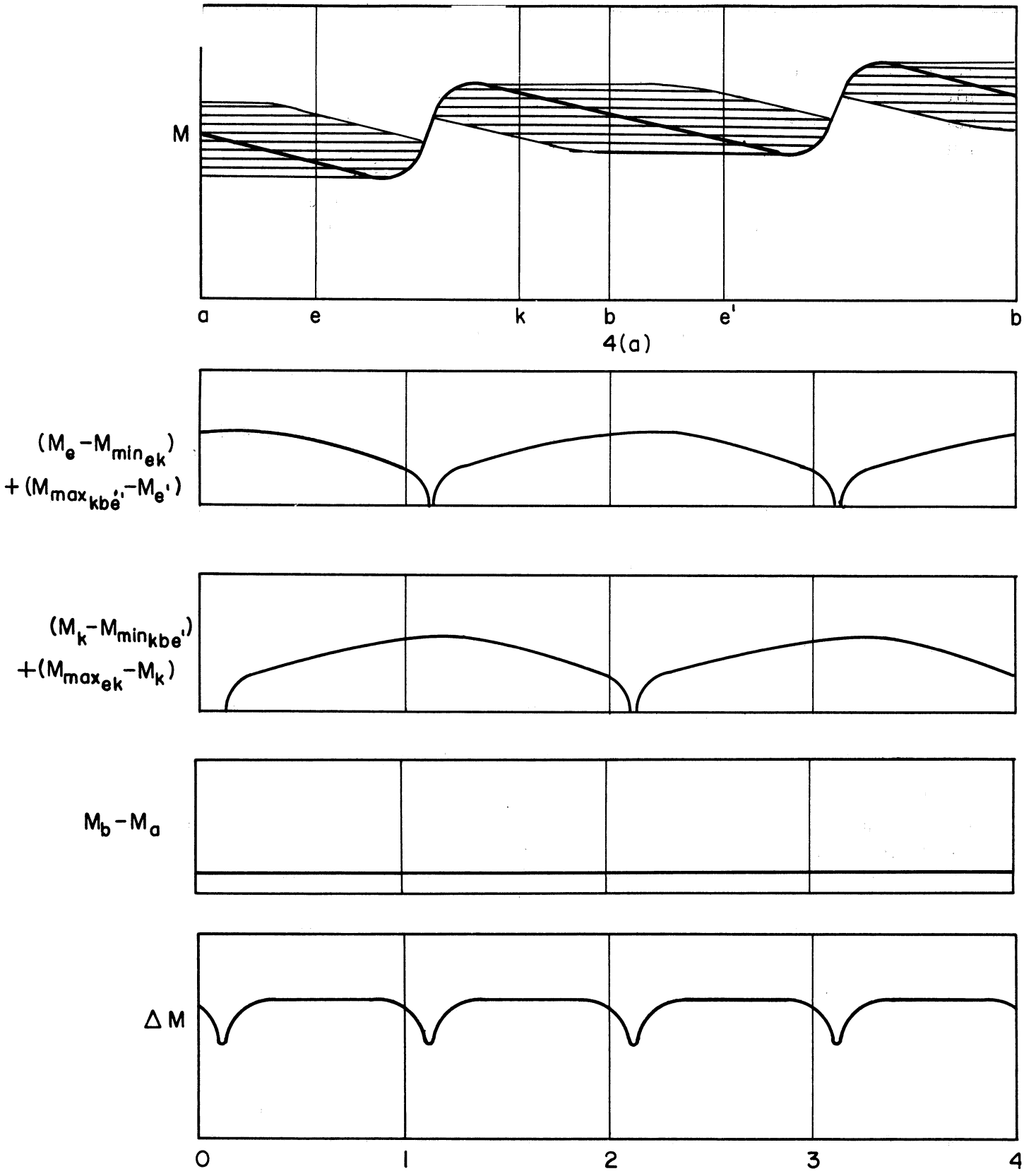
M
a
e
k
b
e'
b
4(a)
$(M_e - M_{min_{ek}})$
$+(M_{max_{kbe'}} - M_{e'})$
$(M_k - M_{min_{kbe'}})$
$+(M_{max_{ek}} - M_k)$
$M_b - M_a$
ΔM
0
1
2
3
4
Test rhombus location ~ rhombus lengths downstream from ab
4(b)

Sketch 4

any rhombus position the four variable terms of equation (D-9) equal the sum of the vertical thicknesses of shaded area at two abscissas of Sketch 4(a) spaced a distance apart equal to half of ab.

Sketch 4(b) shows how the total Mach number variation ΔM is obtained from Sketch 4(a) by adding the shaded areas to the overall Mach number gradient. For any given rhombus location (abscissa of Sketch 4) the top curve of Sketch 4(b) shows the value of the sum of the 2nd and 5th terms of equation (D-9). The next two curves represent the sum of the 3rd and 4th terms, and the 1st term, respectively. The bottom curve represents the total Mach number variation ΔM as the sum of the ordinates of the other three curves.

The application of this type of analysis to real flows introduces two additional sources of error: (1) the flow may not be exactly two-dimensional, and (2) the disturbance waves reflect not from the walls but from the boundary layers. This second effect may be at least partly compensated for by considering the waves to reflect from an appropriate part of the boundary layer.

Summary: The flow in a wind tunnel test section can be determined by static-pressure measurements along the floor or ceiling, or by Mach number or flow-angle measurements along a Mach line. (If the flow is symmetrical, Mach number measurements along the centerline are sufficient.) The greatest difference in Mach number within a test rhombus can be easily determined as a function of rhombus location. This difference must be greater than one-half, but less than one, times the Mach number variation along two rhombus lengths of the floor or ceiling. The analysis does not consider errors due to non-two-dimensional flow or boundary layer modification of disturbance wave strength.

APPENDIX E

CONTOUR TOLERANCES

The effect of a contour defect on the test-section flow can be conservatively approximated by assuming that the expansion and compression waves arising from the defect do not interact with the boundary layers or with themselves. Then the angular deviations of the manufactured contour from the specified curve will be propagated directly into the flow as changes in local-flow angle which will follow the Mach lines into the test section. If the test-section flow-angle deviations due to manufacturing errors are to be kept below a certain value, $\Delta\alpha$, then the deviations in slope of the contour from a smooth curve faired through the specified values must also be less than $\Delta\alpha$.

Where deviations of Mach number or static pressure in the test section are of greater interest than are those of flow angle, the flow-angle deviation corresponding to a given deviation in Mach number, ΔM, or static pressure, Δp, can be found from linear theory as

$$\Delta\alpha = \pm \frac{\sqrt{M^2-1}}{\gamma M^2} \frac{\Delta p}{p} \tag{E-1}$$

$$\Delta\alpha = \mp \frac{\sqrt{M^2-1}}{1 + \frac{\gamma-1}{2} M^2} \frac{\Delta M}{M} \tag{E-2}$$

Once it has been decided what nonuniformities in flow angle due to manufacturing errors may be allowed, the problem arises of how to specify the contour tolerances in order to keep slope errors below this amount, $\Delta\alpha$. This problem will be treated here by assuming the manufacturing errors are sinusoidal, of wavelength L and amplitude $\pm \Delta y_{max}$. The deviation Δy from the desired contour can then be written

$$\Delta y = \Delta y_{max} \sin \frac{2\pi x}{L} \tag{E-3}$$

where x is the distance along the contour from a point where $\Delta y = o$. The maximum error in slope will be

$$\left(\frac{d\Delta y}{dx}\right)_{max} = \frac{2\pi \Delta y_{max}}{L} \left(\cos \frac{2\pi x}{L}\right)_{max}$$

$$= \pm \frac{2\pi \Delta y_{max}}{L} \tag{E-4}$$

so that

$$\Delta\alpha = \pm \frac{2\pi \Delta y_{max}}{L} \tag{E-5}$$

Therefore, the deviation of any point on the contour from a smooth curve through the specified points must not exceed

$$\Delta y_{max} = \pm \frac{L\Delta\alpha}{2\pi} \tag{E-6}$$

Contour defects of semi-height exceeding the above maximum allowable value can be discovered and removed by the usual measuring and manufacturing techniques if they are of sufficiently long wavelength. For controlling shorter wavelength defects, a curvature gage of the type shown in Fig. 2.4 may be used. The reading of such a gage with center contact at a point of maximum curvature of a sine wave is

$$G = 2\Delta y_{max} \left(1 - \cos 2\pi \frac{lg}{L}\right) \tag{E-7}$$

where lg is the distance between the center contact and each of the outer contacts. In terms of $\Delta\alpha$ this is

$$G = \frac{L}{\pi} \Delta\alpha \left(1 - \cos 2\pi \frac{lg}{L}\right) \qquad \text{(E-8)}$$

Thus, slope errors will be less than $\Delta\alpha$ if deviations of the curvature gage reading ΔG from the desired value due to the basic nozzle curvature do not exceed

$$\Delta G_{max} = \frac{L}{\pi} \Delta\alpha \left(1 - \cos 2\pi \frac{lg}{L}\right) \qquad \text{(E-9)}$$

This equation is plotted in Fig. E.1 for gage lengths l_g = 1/4 inch and l_g = 1 inch.

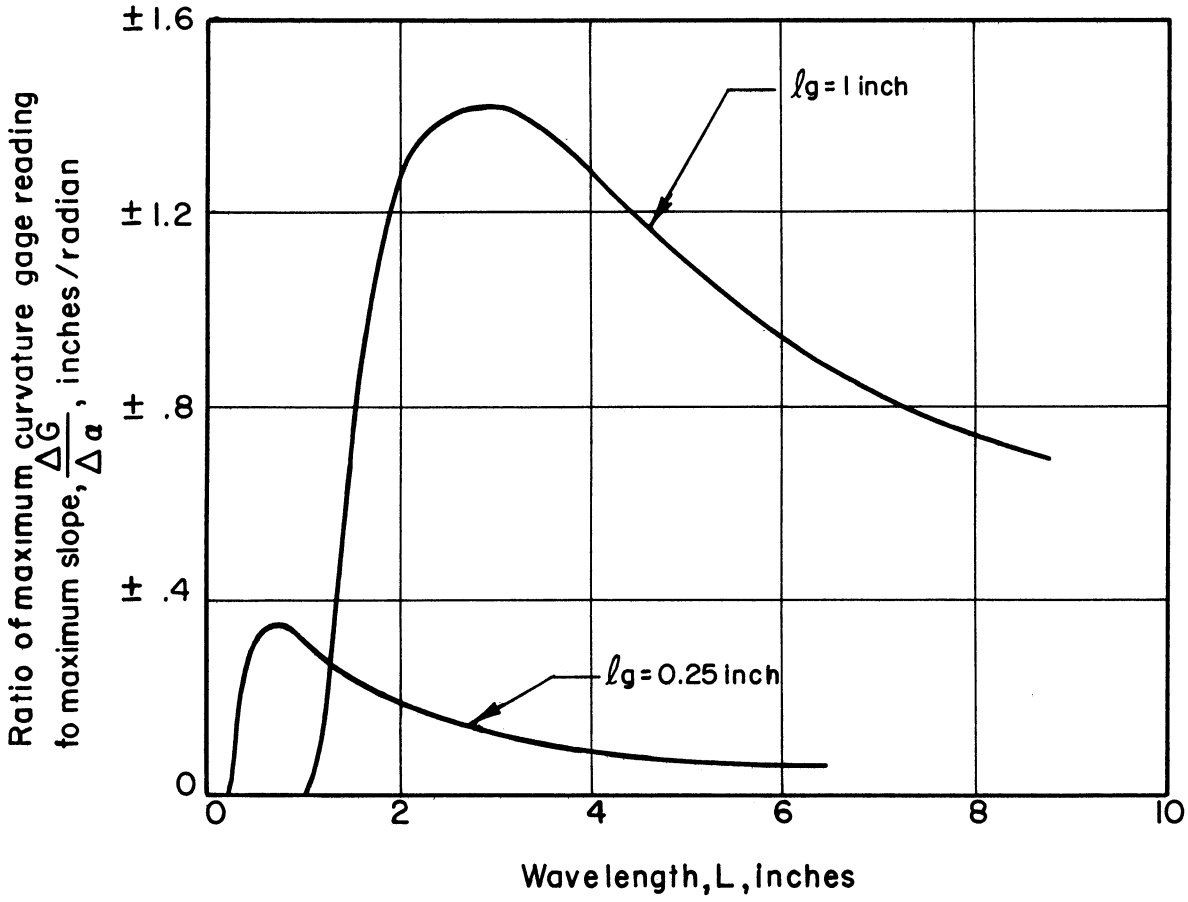

Fig. E.1. Ratio of maximum curvature gage reading on a sine wave to maximum slope of the sine wave, as a function of length of the wave.

It is desirable to eliminate the wavelength as a parameter in contour tolerance specifications. This can be done by observing from Fig. E.1 that for a 1/4-inch curvature gage (l_g = 0.25 inch)

$$(\Delta G_{max})_{0.25} \geqq 0.23\Delta\alpha \text{ for } .4 < L < 1.55, \tag{E-10}$$

and for a 1-inch curvature gage

$$(\Delta G_{max})_1 \geqq 0.80\Delta\alpha \text{ for } 1.55 < L < 7.3, \tag{E-11}$$

and also, using equation (E-6),

$$\Delta y_{max} \geqq 1.16\Delta\alpha \text{ for } 7.3 < L. \tag{E-12}$$

Slope errors can therefore be held to values less than $\Delta\alpha$, for wavelengths greater than 0.4 inches by the following set of tolerances:

$$|\Delta y| \leqq 1.16\Delta\alpha \quad \text{(ordinate tolerance)} \tag{E-13}$$

$$|\Delta G_1| \leqq 0.80\Delta\alpha \quad \text{(1-inch curvature gage tolerance)} \tag{E-14}$$

$$|\Delta G_{0.25}| \leqq 0.23\Delta\alpha \quad \text{(1/4-inch curvature gage tolerance),} \tag{E-15}$$

where the tolerances are in inches and $\Delta\alpha$ is in radians. For $\Delta\alpha$ in degrees these are

$$|\Delta y| \leqq 0.020\Delta\alpha \tag{E-16}$$

$$|\Delta G_1| \leqq 0.014\Delta\alpha \tag{E-17}$$

$$|\Delta G_{0.25}| \leqq 0.004\Delta\alpha \tag{E-18}$$

In order to use the above curvature tolerances it is necessary to determine the correct reading of the curvature gage at every point along the nozzle from the specified coordinates. By simple geometry it can be shown that the gage reading is related to the average radius of curvature R over the portion of the nozzle spanned by the gage, by the equation

$$G = \frac{l_g^2}{R}\left[\frac{1}{2} + \frac{1}{2\left(\cos\frac{l_g}{R}\right)^2}\right] \tag{E-19}$$

The quantity in brackets can be set equal to unity with very small percentage error in G, so that

$$G = \frac{l_g^2}{R} = l_g^2 K \tag{E-20}$$

where K is the curvature. $\left(K \equiv \frac{1}{R}\right)$.

The average curvature K over a portion of the nozzle contour corresponding to an interval 2 Δx along the x-coordinate axis is very nearly

$$K = \frac{\Delta^2 y}{(\Delta x)^2\left[1 + \left(\frac{\Delta y}{\Delta x}\right)^2\right]^{3/2}} \qquad \text{(E-21)}$$

where Δy is the increment in y associated with Δx, and $\Delta^2 y$ is the difference between the Δy's of the two adjacent Δx intervals. Then the reading of a curvature gage having $l_g = \Delta x$ can be expressed in terms of the coordinates, by combining equations (E-20) and (E-21), as

$$G = \frac{\Delta^2 y}{\left[1 + \left(\frac{\Delta y}{\Delta x}\right)^2\right]^{3/2}} . \qquad \text{(E-22)}$$

From this equation the correct readings of a curvature gage of gage length l_g can be calculated from the first and second differences in the y-coordinates at interval l_g.

APPENDIX F

DIFFUSER PERFORMANCE

The nozzle model was originally equipped with an adjustable supersonic diffuser. The flow through this diffuser was bounded on the bottom by a flat plate extension of the lower nozzle block, on the sides by parallel flat walls, and on the top by two flat plates hinged together. The upstream plate was 25 inches long; the downstream plate, 37 inches. The hinge point between these plates could be lowered, reducing the angle between the plates to less than 180°, and forming a throat. This throat was 37 inches downstream of the nozzle exit.

The entrance cross section of the adjustable diffuser was 4 inches wide and from 4- to 5-1/2 inches high, depending on the nozzle configuration. The exit of the adjustable diffuser was 4 by 5 inches. A 5-foot-long transition section continued the subsonic diffusion to the 8-inch-diameter butterfly valve.

The performance of the adjustable diffuser described above, in conjunction with the empty tunnel with jacks set for the theoretical contours, was determined by measuring the vacuum tank pressure at the moment of flow break-up. The resulting overall pressure ratios required to maintain supersonic flow are shown in Fig. F.1 for two conditions: (1) diffuser throat wide open, and (2) diffuser throat closed to optimum position after starting. Minimum diffuser throat-to-test-section area ratios for starting and for maintaining flow are shown in Fig. F.2.

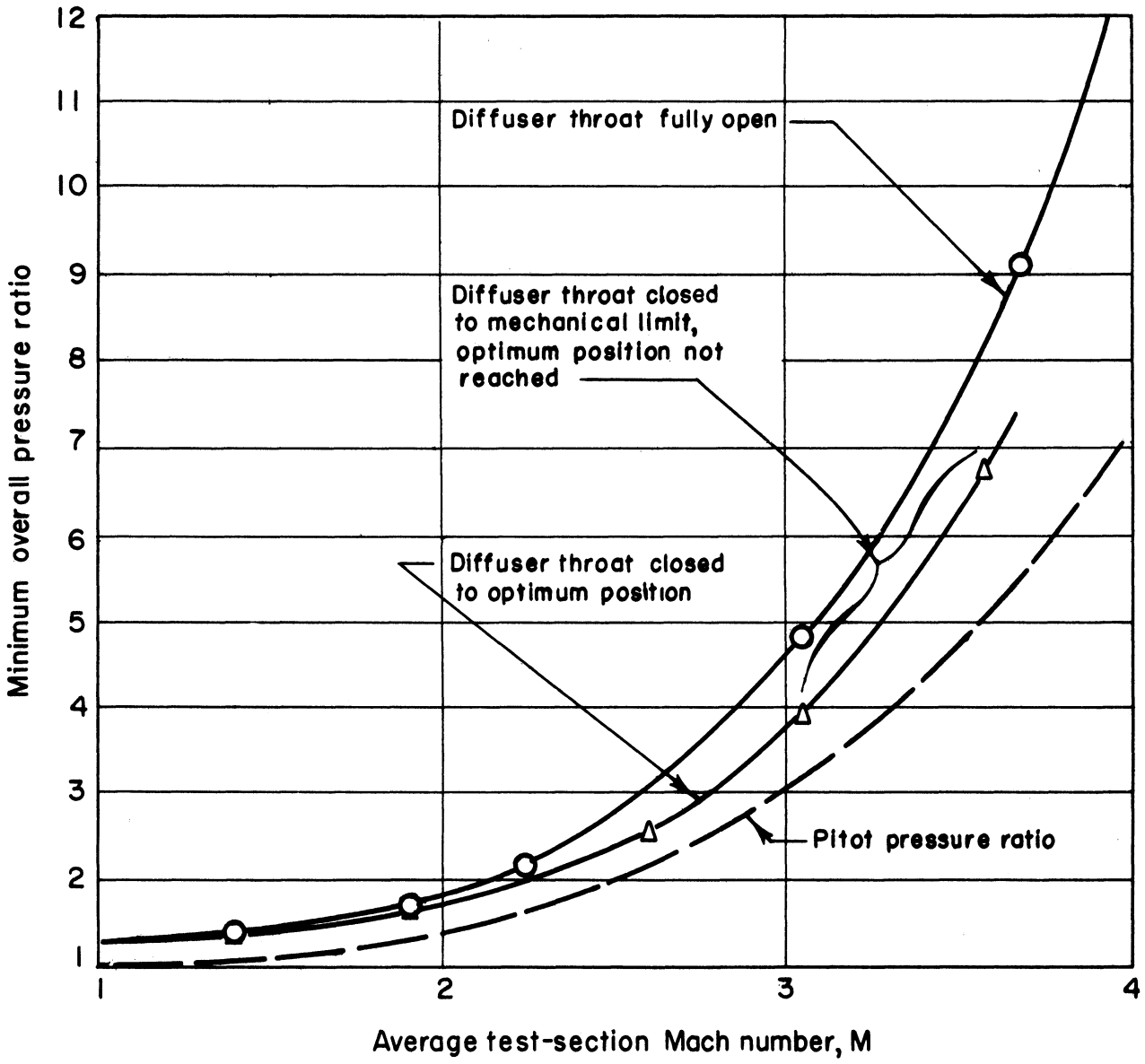

Fig. F.1. Minimum overall-pressure ratios for two diffuser conditions. Nozzle with theoretical inviscid contours.

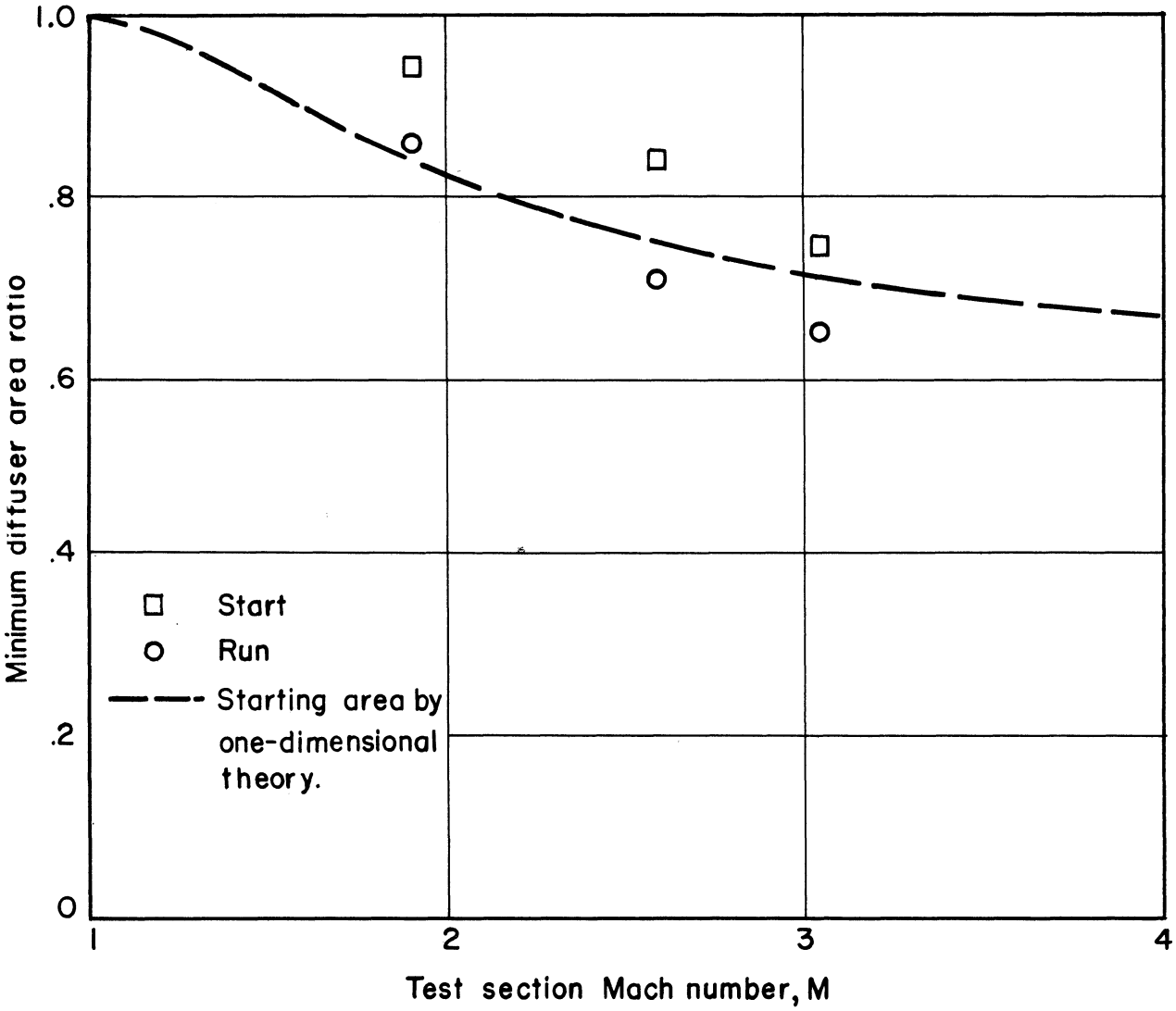

Fig. F.2. Approximate minimum diffuser area ratios for starting and for running. 4- by 4-inch asymmetric adjustable nozzle with original contours. Tunnel empty.

The overall pressure ratios of Fig. F.1 with diffuser throat closed to optimum position after starting are somewhat higher than those of a pitot tube. It is probable that this performance could be improved by modifications of the adjustable diffuser geometry.